

Using A Physics-Based Model to Characterize Spotting Potential for Protection of the Wildland Urban Interface

Final Report: JFPS Project Number 07-1-5-01

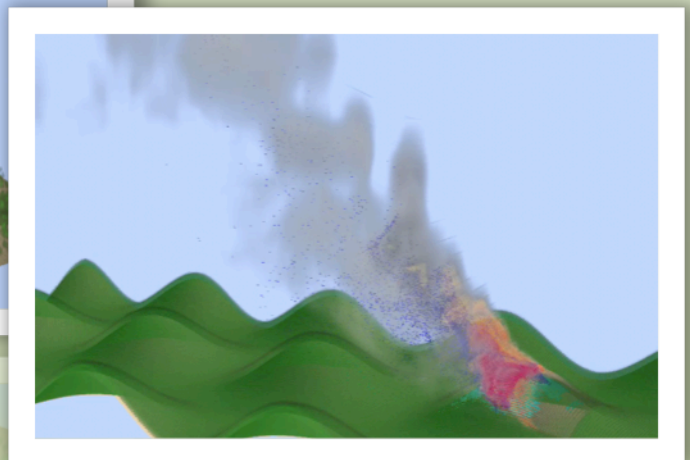
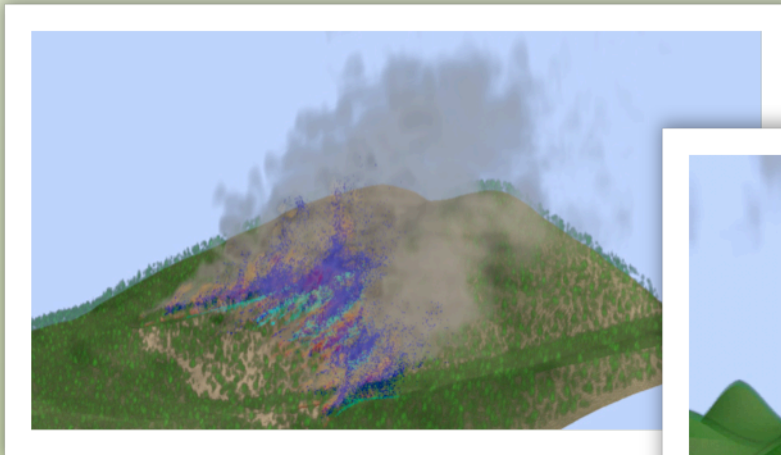
Principal Investigator: **Dr. Rodman R. Linn**

Computational Earth Sciences, Earth and Environmental Science Division,
Los Alamos National Laboratory, MS D401, EES-16, Los Alamos National Laboratory, Los
Alamos, NM 87545; Phone: 505-665-6254; email: rrl@lanl.gov

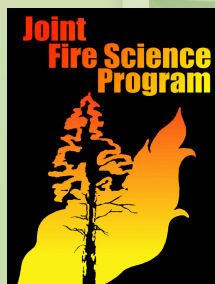
Federal Cooperator: **Dr. Carolyn H. Sieg**

Rocky Mountain Research Station, USDA Forest Service, 2500 South Pine Knoll, Flagstaff,
AZ 86001; Phone: 928-556-2151; email: csieg@fs.fe.us

Additional Federal Collaborators: **Dr. Eunmo Koo** (LANL), **Judith Winterkamp** (LANL)



This research was sponsored by the Joint Fire Science Program. For further information, visit www.firescience.gov.



1. Abstract

To provide critical spotting information to fire managers and the developers of operational wildfire behavior models, a physics-based spotting model has been developed and used to characterize potential spotting hazard in complex wildland urban interface (WUI) fires. The spread of large-scale fires is a result of two types of phenomena: contiguous spread and spotting. Spotting is the phenomenon by which burning material, called firebrands, are lofted by the plume, transported via the fire-influenced wind field, and deposited to ignite new fires ahead of the contiguous fire front. Spotting behavior depends on the strong coupling between fire, atmosphere, topography, and fuels and is therefore difficult to characterize without adequate methods of accounting for this coupling. In order to predict spotting, the physical firebrand model has been integrated into HIGRAD/FIRETEC, a premier physics-based model for the prediction of contiguous fire spread. Incorporating the firebrand model into HIGRAD/FIRETEC provides a mechanism to predict spotting locations in a wide range of conditions including rugged terrain, gusty winds, and non-homogeneous fuels. The coupled effects of fuel types/conditions, fuel heterogeneity, atmospheric wind speed/gust/turbulence, topography, and human-made structures could be studied through the HIGRAD/FIRETEC_SPOT model and be characterized. It is found that the flame/plume structure with wind conditions around fire is critical for predicting spotting behavior. It is recommended to study of plume structure/wind patterns and critical factors on them such as topology and atmospheric conditions for further firebrand research. The knowledge obtained from this project and further investigation will be practical information for fire and land management personnel.

2. Background and purpose

Historical examples of large-scale WUI fires have shown the role of firebrands and spotting. These examples include the 1961 Bel-Air Fire (Wilson 1962), the 1991 Oakland Hills Fire (Pagni 1993), and the 2000 Cerro Grande Fire (US National Park Service 2000). The 1961 Bel-Air Fire started as a wildfire and spread to the structures in an urban area. This fire showed a typical WUI fire spread mechanism: firebrands ignited the roofs of the structures. The Santa Ana winds in Southern California transported the firebrands and contributed to the ignition of the

structures. The 1991 Oakland Hills Fire, another example of a spotting-dominated fire, cost more than 1.5 billion USD and killed 25 people. Recently, the 2000 Cerro Grande Fire started as an escaped prescribed burn. It burned 235 structures, 48000 acres, and threatened the Los Alamos National Laboratory. Significant spotting was observed in all of these WUI fires. Discontinuous fire spread due to spotting is not a well-understood wildfire behavior and is very unpredictable, so even well trained firefighters can be victims of spotting. In the 1994 South Canyon Fire in Colorado (Butler *et al.* 1998) firefighters were trapped by spot fires, causing the death of 14 firefighters.

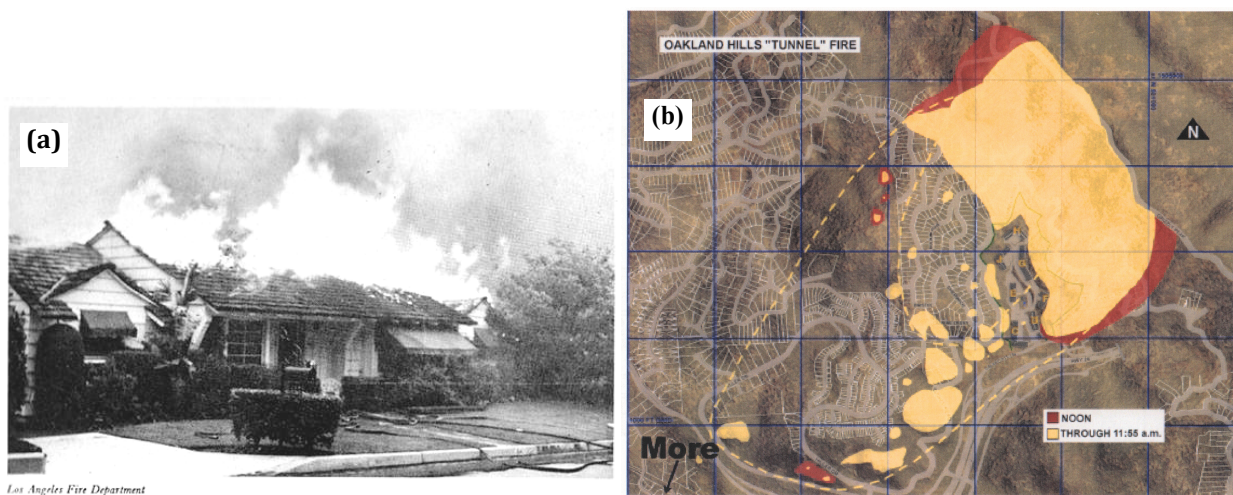


Figure 1. Spotting in wildland urban interface fires: (a) Ignition of the roof by the impact of firebrands in the 1961 Bel-Air Fire. (From Fig. 5, p.256, (Wilson 1962)). (b) A map of the 1991 Oakland Hills Fire. Blue lines are California State Grid with 300m spacing. The colored area indicates where the fire had spread by noon on 21 October 1991. The map indicated there were more spot fires across Highway 24, a 4-lane expressway; firebrands leapt across the highway and ignited structures. This map was developed from eyewitness reports, emergency crew accounts, and 911 phone calls by Dave Sapsis of the University of California at Berkeley (Woycheese 2000).

Developing a reliable tool for predicting spotting behavior is an essential part of developing a fire behavior model in WUI. This new spot behavior model should be based on physics, and incorporated into a physics-based contiguous fire spread model. It is critical that the combined tool be able to address the coupling between fire, atmosphere, topography, and fuel structure. HIGRAD/FIRETEC is designed so that it is well-suited to investigate these couplings. There are other physics-based wildfire models that are two-dimensional or currently can only be used on flat ground. HIGRAD/FIRETEC is the only physics-based wildfire behavior model that

simulates the physical processes involved in fire/atmosphere/topography/fuels coupling in three dimensions on landscape scales. As a preliminary demonstration of the coupling of the spotting model with HIGRAD/FIRETEC, firebrand transport in several simple wildfire scenarios has been studied as a post-processor of HIGRAD/FIRETEC (Koo 2008; Koo *et al.* 2007).

It is critical that fire managers be aware of situations in which fire/atmosphere/topography coupling can produce strong spotting potential, and where the spot fires are likely to break out. This is important to protect civilians and infrastructures by allowing educated decisions about the allocation of resources to attend to spot fires as they occur, designating evacuation routes and making the public aware of the dangers of shelter-in-place scenarios. The knowledge that will be accumulated through this study of spotting phenomena with HIGRAD/FIRETEC_SPOT will help improve current operational models and will be summarized in the form of guidelines, scenario descriptions for fire managers and homeowners in WUI and rules for simplified operational tools for spotting.

Since Tarifa (1965a) experimented on firebrand combustion in a wind tunnel in the 1960s, spot fire research has been focused on the transport of a firebrand. The maximum spot fire distance for a single firebrand has been used to describe the spotting threat quantitatively. Tarifa studied the dynamics of a burning firebrand in constant wind and found that it only takes 2 to 3 seconds to adjust its velocity to terminal velocity, which is much shorter of a period of time than the lifetime of a burning firebrand. Therefore, he assumed that a flying firebrand moves with its terminal velocity. This terminal velocity approximation has been applied in almost all firebrand research after Tarifa and is valid if the wind fields remain constant during the firebrand's flight. With simplified plume models and constant wind conditions, Tarifa estimated the maximum spotting distance (Tarifa *et al.* 1965a). Lee and Hellman (1969) analyzed the motion of firebrands in the fire whirl and Muraszew (Muraszew and Fedele 1976) suggested statistical models for firebrand generations and ignition over firebrand landings. Albini (1979) developed a predictive model for the maximum spot fire distance of firebrands from a torching tree. Albini expanded his model to other firebrand sources in wildfires, such as wind-driven surface fires (Albini 1983a) and burning wood piles (Albini 1981). Albini's model is now incorporated into the current operational models, BEHAVEPLUS and FARSITE. In order to estimate the

maximum spotting distance, he assumed that firebrands start to propagate downwind after the flame/plume structure collapses, which means that the main fire is extinguished prior to starting to transport firebrands. Recently, Woycheese and Pagni (2001; 1999) studied the maximum spotting distance of combusting firebrands with non-dimensionalization. These theoretical studies focus on the trajectory of a single firebrand in simplified flame/plume structures. The insights gained through these studies will be a basis for the proposed work, which focuses on simulations of multiple firebrands in complex and realistic wind fields induced by wildfires and WUI fires.

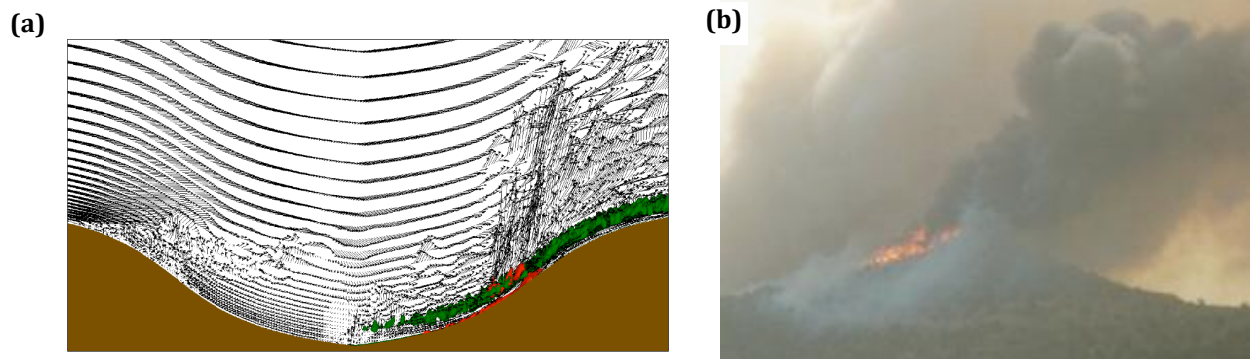


Figure 2. Coupled effects of fire/topography/fuel on fire-induced wind and fire spread in wildland fire: (a) This is an image from a HIGRAD/FIRETEC simulation of wildfire in a canyon. Each arrow is a wind velocity vector. Due to the topography, a recirculation coming up under the wind separates the flow from the ground as shown on the left. The vegetation change at the bottom of the canyon also disrupts the flow. The coupled fire/atmosphere/topographic flow seen on the right results in a jet forming a strong plume that is capable of affecting firebrand transport. **(b)** This is an image from the Long Canyon Fire in Colorado in 2002. (From <http://www.ens-newswire.com/ens/jun2002/2002-06-10-06.asp> image courtesy USDA Forest Service). In (b), the same flow pattern as (a) above on the upslope of the contiguous fire spread can be observed with smoke. After an upslope contiguous fire front hits the top of the hill and becomes a downslope spread, the spread rate generally decreases significantly. However, the strong jet induced by the fire and influenced by topography, as shown in (a), can loft and transport substantial firebrands to the downhill slope.

3. Study description and location

The study was conducted at Los Alamos National Laboratory (LANL) with numerical simulations. LANL is uniquely qualified to perform this research due to its widely recognized physics-based coupled fire/atmosphere wildfire model HIGRAD/FIRETEC, computational resources, and expertise in science-based predictions. In order to adequately characterize the impacts of atmospheric conditions, fuel structure, and topography on the probable landing

locations of firebrands a very large set of computationally intensive simulations has been performed using the computer resources at LANL. These simulations use the massively parallel systems available in order to resolve critical time and space scales that are important in this problem.

A. Firebrand model

Though firebrands can have a wide variety of complex shapes in reality, the modeling approach for this study focuses on firebrands that can be loosely represented by two simple firebrand shapes with defined orientations, a disk and a cylinder. This subset of possible shapes is used for model and computational tractability, with the idea that these shapes are fairly representative of a large fraction of firebrands from natural and WUI fires. For this study, firebrand models are developed for the evolution and flight characteristics of thin disk and long cylindrical firebrands. These models include elements describing the combustion and resulting evolution of the shape of firebrands as well as elements modeling the force balance and resulting lift and drag properties of the firebrands. In order to assess the impact of the terminal velocity assumption, force balance models with and without this assumption are developed and tested. The formulations and their implications are described in this section.

Force Balance with terminal velocity assumption

Disks and cylinders have the same basic geometry with different height-radius ratios. Thus, their volume can be expressed in the same way, $(vol) = \pi r^2 h$ where h is the thickness or length and r is the radius. The cross-section area, which is related to their primary orientation to the wind, could be either πr^2 or $2rh$. Their orientation with respect to the relative wind must be considered differently based on the difference in their free-falling stability. Tarifa *et al.* (1965a) found in free-falling tests that disk and cylindrical firebrands' velocities remain reasonably stable at specific orientations during flight. When the height-radius ratio is less than approximately 0.5 (disk) the cross-section area should be πr^2 . When the height-radius ratio is greater than approximately 5 (cylinder) the cross-section area should be $2rh$, as shown in Fig. 3. Assuming the firebrand is always in the position of maximum drag disregards tumbling and wobbling, and could lead to over prediction of the wind's ability to lift and carry firebrands. The no tumbling or wobbling approximation provides a worst-case estimate of maximum spot fire distances.

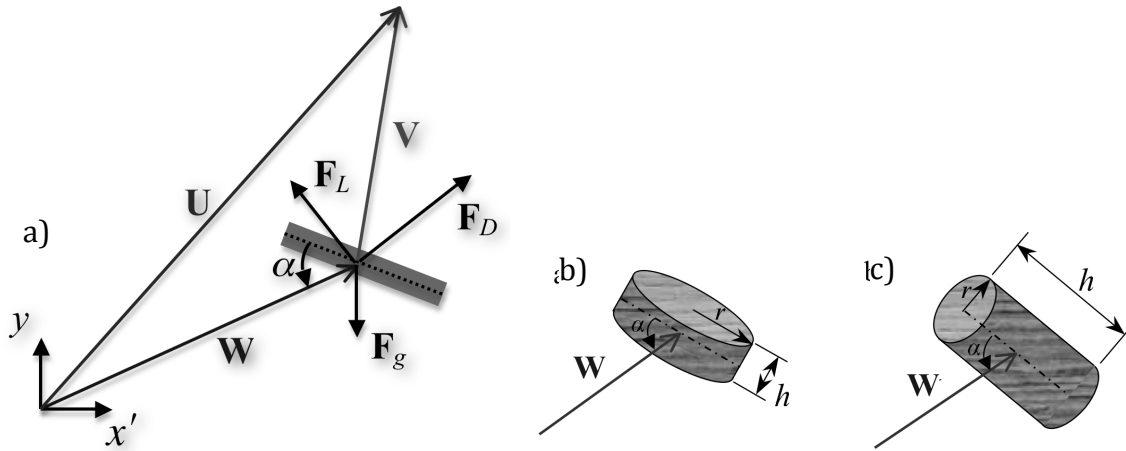


Figure 3. a) Force balance schematic for a firebrand moving at terminal velocity with respect to the wind: a firebrand model with orientation. e.g., b) a disk or c) a cylinder. The angle of attack is defined from different reference lines as shown.

Figure 3a shows a force balance schematic for a disk or cylindrical firebrand in a wind reference frame. z is the vertical direction, and x' is the horizontal direction aligned with the local wind velocities. In other words, the firebrand is at an instant where it is immersed in a flow that can locally be described in an x' - z plane, but the x' direction is specific to that point in time and space. In this context, the three-dimensional forces acting on the firebrand also lie within the two-dimensional x' - z plane.

This two-dimensional representation assumes that the firebrand is always perpendicular to the x' - z plane that contains the instantaneous relative wind velocity vector. This is consistent with the concept of ignoring tumbling or wobbling. \mathbf{W} is the wind velocity relative to the firebrand, which is generally different from the flow velocity relative to the ground, \mathbf{U} , or the firebrand velocity relative to the ground, \mathbf{V} . The wind velocity relative to the firebrand, subsequently called relative velocity, is equal to the difference between the local winds and the actual velocity of the firebrand, $\mathbf{W} = \mathbf{U} - \mathbf{V}$. α is the angle of attack, which is the angle between \mathbf{W} and a line defining the firebrand orientation (shown as a dotted line).

The firebrand is acted upon by its own weight, which is the gravity force, \mathbf{F}_g , and the pressure force induced by the flow around the firebrand. The pressure force can be decomposed into two component forces: the drag force, \mathbf{F}_D , which is aligned with the relative wind, and the lift force,

\mathbf{F}_L , which is normal to the relative wind. Thus there are three forces acting on a firebrand in flight: gravity force, drag force and lift force. These forces are determined as follows:

$$\text{Drag force: } \begin{cases} F_{D,x'} = \frac{1}{2} A_c \rho_a C_D |\mathbf{W}| W_{x'}, & (a) \\ F_{D,z} = \frac{1}{2} A_c \rho_a C_D |\mathbf{W}| W_z; & (b) \end{cases} \quad (1)$$

$$\text{Lift force: } \begin{cases} F_{L,x'} = -\frac{1}{2} A_c \rho_a C_L |\mathbf{W}| W_z, & (a) \\ F_{L,z} = \frac{1}{2} A_c \rho_a C_L |\mathbf{W}| W_{x'}; & (b) \end{cases} \quad (2)$$

$$\text{Gravity force: } \begin{cases} F_{g,x'} = 0, & (a) \\ F_{g,z} = -mg = -\rho_s (\text{vol}) g; & (b) \end{cases} \quad (3)$$

where A_c is the cross-section firebrand area (or projected area), ρ is the density, C_D is a drag coefficient, C_L is a lift coefficient, $(\text{vol}) =$ volume of firebrand, m is the mass of the firebrand, g is the acceleration due to gravity and the subscripts a and s indicate air and solid. Figures 2-b) and 2-c) show a disk firebrand and a cylinder firebrand with different definitions of the angle of attack. For the disk, α is the angle between the plane and \mathbf{W} and cross-section area is πr^2 . For the cylinder, α is the angle between its axis and \mathbf{W} . and cross-section area is $2rh$. Drag and lift coefficients are assumed to be the two components of the normal pressure coefficient, C_N (Hoerner 1958):

$$\begin{aligned} C_D &= C_N \sin \alpha, & (a) \\ C_L &= C_N \cos \alpha. & (b) \end{aligned} \quad (4)$$

These velocity vector and force conventions were first used for firebrand transport research by Tarifa *et al.* (1965a; 1967; 1965b), and formed the basis of most firebrand research that followed these early works. Tarifa also established the important assumption that firebrands in flight travel at their terminal velocities with respect to the wind. When a free-falling object is at its terminal

velocity in a static homogeneous wind field, its acceleration is zero because the sum of the external forces (pressure and body) acting on the object is assumed to be zero, or:

$$\frac{d}{dt}(m\mathbf{V}) = \sum_i \mathbf{F}_i = 0 \quad (5)$$

For the sum of forces defined by equations (1,2,3, and 4), the terminal velocity approximation yields:

$$\frac{1}{2}A_c\rho_a|\mathbf{W}|C_N(W_{x'}\sin\alpha - W_z\cos\alpha) = 0 \quad (a)$$

$$\frac{1}{2}A_c\rho_a|\mathbf{W}|C_N(W_z\sin\alpha + W_{x'}\cos\alpha) - mg = 0 \quad (b) \quad (6)$$

Equation (6) is the governing equation of firebrand dynamics for all shapes under the terminal velocity assumption. For spheres, which have no preferential direction, $\alpha = 90^\circ$.

The relative wind velocity \mathbf{W} can be solved from the force balance equation (5). For disks, the components of the relative wind velocity are:

$$W_{x'} = \cos\alpha \cdot \sqrt{2\left(\frac{\rho_s}{\rho_a}\right)\left(\frac{hg}{C_N}\right)}, \quad W_z = \sin\alpha \cdot \sqrt{2\left(\frac{\rho_s}{\rho_a}\right)\left(\frac{hg}{C_N}\right)}; \quad (7)$$

and for cylinders,

$$W_{x'} = \cos\alpha \cdot \sqrt{\pi\left(\frac{\rho_s}{\rho_a}\right)\left(\frac{rg}{C_N}\right)}, \quad W_z = \sin\alpha \cdot \sqrt{\pi\left(\frac{\rho_s}{\rho_a}\right)\left(\frac{rg}{C_N}\right)}. \quad (8)$$

Since drag forces depend strongly on shape, C_N is found for each case using preexisting data.

Many experiments for determining C_N for simple body shapes like disks and cylinders have been performed by various researchers, such as the experiments summarized in Fig. 4, which are found in (Hoerner 1958). Fig. 4a shows that for disks, C_N is constant at 1.17 if the angle of attack is between 35° and 90° . In Fig. 4b, C_L and C_D for cylinders are shown. Note that C_L and C_D are functions of the angle of attack and C_N in equation (6) whereas C_L and C_D in Fig. 4b follow the cross-flow principle defined by $C_N = C_{N,basis} \sin^2\alpha$, where $C_{N,basis}$ is the pressure coefficient when

$\alpha = 90^\circ$. The friction drag coefficient of the cylinder, 0.02 in Fig. 3b, is ignored here. When the height-to-radius ratio is around 10, $C_{N,basis} \approx 0.7$ (White 1999). As the height-to-radius ratio goes to infinity, $C_{N,basis} \approx 1.1$, as shown in Fig. 3b (Hoerner 1958).

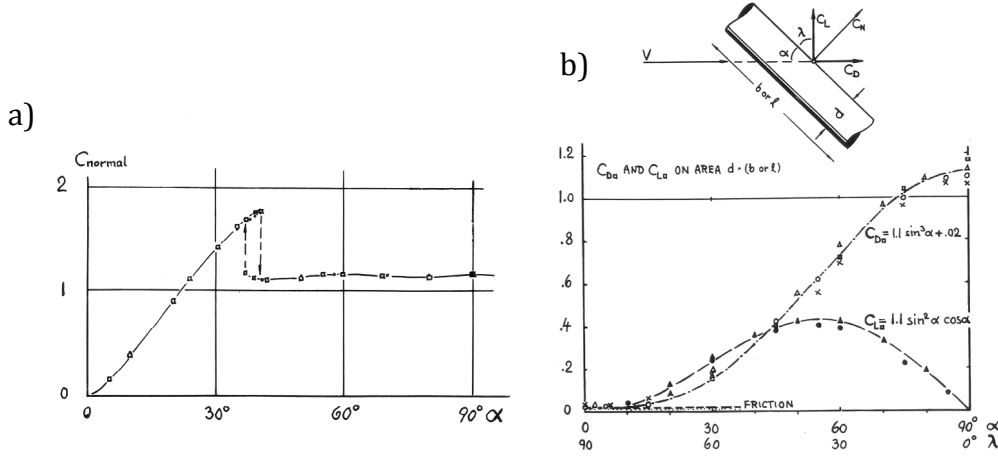


Figure 4. Normal pressure coefficient C_N vs. the angle of attack α for (a) disks and (b) infinite cylinders such as wires and cables. From Fig. 29(a), p.3-16 and Fig. 18, p.3-11, in (Hoerner 1958).

With the equations listed above, the firebrand velocity, \mathbf{V} , can be calculated from \mathbf{W} for a given local value of \mathbf{U} , which is obtained at each position from HIGRAD/FIRETEC. The position of a firebrand can be traced by obtaining the distance traveled during Δt by integrating over time:

$$\Delta x = \int_t^{t+\Delta t} (U_x - W_x) dt, \quad \Delta z = \int_t^{t+\Delta t} (U_z - W_z) dt. \quad (9)$$

Again, with the terminal velocity assumption, there is an assumed balance between the instantaneous/local pressure forces and body forces. For numerical implementation purposes, this is expanded to say that this balance remains constant over the duration of a time step, Δt . After each time step, a new firebrand position and evolved wind field provides a new \mathbf{U} and thus a new \mathbf{W} is calculated.

Forces and acceleration without the terminal velocity assumption

The model described above was based on the terminal velocity assumption established by Tarifa from his observations of firebrand burning tests in a wind tunnel (Tarifa *et al.* 1965a). Tarifa observed that it took only two to three seconds for a firebrand to adjust its velocity to its terminal

velocity in the wind tunnel. He considered two to three seconds of startup time as a short enough time to be ignored. This time decreases as the size or density of the firebrand decreases. Thus, Tarifa assumed that a flying firebrand adjusts to its terminal velocity immediately. The terminal velocity postulate has been assumed to be true in many other studies (Albini 1979; Albini 1981; Albini 1982; Albini 1983a; Albini 1983b; Himoto and Tanaka 2005; Lee and Hellman 1969; Lee and Hellman 1970; Muraszew 1974; Muraszew and Fedele 1976; Muraszew and Fedele 1977; Muraszew *et al.* 1975; Woycheese 1996; Woycheese 2000; Woycheese *et al.* 1998; Woycheese *et al.* 1999). However, this assumption implies that the time scale of the local wind change is larger than the start up time (two to three seconds for the tested firebrands). There are two basic ways that the local winds change around a firebrand: 1) the winds evolve in a transient manner; or 2) the firebrand moves from a location with one wind condition to another with a different wind condition. The time scale of the local wind change therefore depends on the spatial heterogeneity of the wind field and the velocity of the firebrand and/or the rate at which the velocity field evolves. In the presence of a turbulent plume emanating from a fire, the time scales of wind change could be much shorter than two seconds, especially near the edge of the plume. If the wind speed keeps changing, then a firebrand will try to adjust its velocity to its terminal velocity. However, the wind could change again before the firebrand reaches terminal velocity, so the adjustment process (acceleration/deceleration) would be continuous.

Without the terminal velocity assumption, the terms in the momentum equations, equation (5), become non-zero as seen in equation (10), where the i index indicates the three normal coordinates x , y , and z with x and y defining the horizontal plane and z the vertical. Without the terminal velocity assumption, the time dependence of the mass and velocity of the firebrand is essential for the estimation of the firebrand velocity, \mathbf{V} :

$$\frac{d}{dt}(m\mathbf{V}) = \sum_i \mathbf{F}_i \neq 0 \quad (10)$$

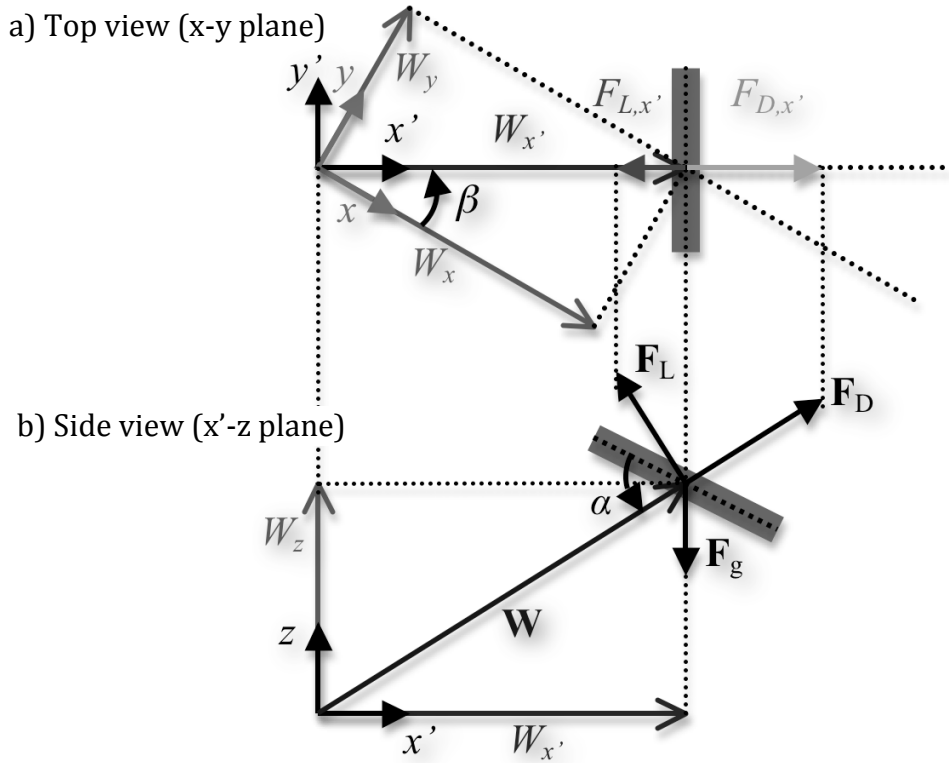


Figure 5. Firebrand schematic in 3-D. a) top view on x-y plane and b) side view on x'-z plane. x' and y' are the principal directions of relative wind; x and y are normal static reference coordinate axes on the horizontal plane, which are used in simulations, and z is in the vertical direction.

Discarding the terminal velocity assumption means that the relative wind vector and the firebrand velocity vector are no longer co-planer on the x' - z plane. This is because the firebrand may have a velocity imparted on it from an earlier moment that has a component perpendicular to this plane. One way to think about this is that the firebrand has a decaying memory of previous wind fields it has experienced. Over an extended time of exposure to a wind field with only x' - z components, any perpendicular velocities will diminish and the firebrand will approach terminal velocity. As shown in Fig. 5a, the firebrand's orientation is assumed to be normal to the relative wind on the horizontal plane because a firebrand is assumed to have no side-lift force and wobbling/tumbling is still being ignored. The implicit assumption that occurs with this treatment is that the orientation of the firebrand reacts in shorter time-scales than the changes in wind direction.

Without the terminal velocity approximation, the angle between the relative wind velocity and the static reference horizontal x -axis, β , is defined in equation (11). Note the four expressions in

equation (11) have the same value, zero, under the terminal velocity assumption. The expressions in terms of \mathbf{U} and \mathbf{V} are included in order to remind the reader that without the terminal velocity approximation the orientation of \mathbf{W} , the relative velocity of the wind with respect to the firebrand, is usually not the same as the direction of the local wind velocity, \mathbf{U} , or the firebrand velocity, \mathbf{V} .

$$\beta \equiv \tan^{-1}\left(\frac{W_y}{W_x}\right) \neq \tan^{-1}\left(\frac{U_y}{U_x}\right) \neq \tan^{-1}\left(\frac{V_y}{V_x}\right) \quad (11)$$

In the horizontal plane, the principal directions of the relative wind, x' and y' , are defined by the angle of β , as seen in Fig. 6a. The relative wind velocities in the principal directions are:

$$\begin{cases} W_{x'} = U_{x'} - V_{x'} = \sqrt{W_x^2 - W_y^2} \\ W_{y'} = U_{y'} - V_{y'} = 0 \end{cases} \quad (12)$$

Note that:

$$\cos \beta = \frac{W_x}{W_{x'}} = \frac{W_x}{\sqrt{W_x^2 + W_y^2}}, \quad \sin \beta = \frac{W_y}{W_{x'}} = \frac{W_y}{\sqrt{W_x^2 + W_y^2}}. \quad (13)$$

The forces acting on a firebrand in equations (1, 2, 3, and 4) are actually in vertical direction, z , and the principal direction, x' , as shown in Fig. 5b. The angle of attack between the relative wind vector and the plane containing the disk or the axis of the cylinder is defined by α .

With the terminal velocity assumption, the firebrand orientation is normal to the firebrand velocity and the absolute wind velocity because the directions of the absolute wind vector, \mathbf{U} , the firebrand velocity vector, \mathbf{V} , and the relative wind vector, \mathbf{W} , are in the same plane. However, without the terminal velocity assumption, these vectors have different directions even with no side-lift force assumption.

Combustion and mass loss models

The combustion process changes firebrands' shapes and densities, which are parameters that affect firebrand dynamics. Tarifa measured combustion effects on firebrand dynamics in wind tunnel experiments, and then used his data in his trajectory calculations (Tarifa *et al.* 1965a;

Tarifa *et al.* 1967). Muraszew did similar experiments but focused on density changes rather than shape changes (Muraszew and Fedele 1976). The current study makes the simplifying assumption that lofted firebrands are already dried out and charred, and so do not change in density while in flight. The density of charred wood, 300 kg m^{-3} , is assumed throughout the firebrand trajectory discussions that follow.

For the current study the wood is also assumed to be a homogenous solid, and the mass loss is assumed to be uniform on any burning surface so that it decreases the height or radius of the disk or cylinder. This is not how firebrands actually burn, because woody material is heterogeneous and is not isotropic. In addition, wood is pyrolyzed by heat supplied by heterogeneous (glowing) combustion of the wood on the outer surface of the firebrand or by the diffusion flame enveloping the firebrand (Albini 1979). The pyrolysis of a solid is a surface or volumetric chemical process (Tse and Fernandez-Pello 1998), but these pyrolyzed volatiles tend to flow along the grain, so the regression tends to happen along the grain orientation. Thus, real firebrands tend to loose mass in grain directions more easily than in the direction perpendicular to grains. However, as Tse and Fernandez-Pello (1998) noted, combustion modeling is difficult without the assumption of uniform regression.

For this study, firebrands are assumed to be in flaming combustion rather than glowing combustion, so diffusion flame analyses are used to determine the regression rates. A boundary layer diffusion flame analyses is used for cylindrical and disk firebrands, whereas the droplet-burning law was used in previous work for spherical firebrands (Fernandez-Pello 1982; Turns 2000; Woycheese 2000; Woycheese *et al.* 1999). The development of the boundary layer diffusion flame analyses relies on Pagni's classic diffusion flame analyses (Pagni 1981) to obtain mass fluxes at the fuel surface, which are equivalent to the mass loss rates from the firebrand. They are found as functions of the Reynolds number, Re , based on the relative wind speed, \mathbf{W} , and the firebrand's size; Spalding's mass transfer number (Spalding 1953), B ; and the mass consumption number, γ . B and γ are defined as in (Pagni 1981):

$$B \equiv \frac{QY_{o,\infty}/\nu_o M_o - h_w}{L}, \quad \gamma \equiv \frac{Y_{o,\infty} \nu_f M_f}{Y_{fw} \nu_o M_o}. \quad (14)$$

where Y denotes the mass fraction, ν denotes the stoichiometric coefficient, M denotes the molecular weight, Q is the energy released by the combustion of ν_f moles of gas phase fuel, h_w is the specific enthalpy at the fuel surface and L is the effective latent heat of pyrolysis. For subscripts, o is oxygen, f is fuel, w is the value at the fuel surface (or wall), and ∞ is a value far from the fuel surface. Using the stoichiometric ratio, s , and rearranging variables, the mass consumption number can be denoted as,

$$\gamma = \frac{sY_{o,\infty}}{Y_{f,w}}, \quad \text{where } Y_{f,w} = \frac{BY_{f,t} - sY_{o,\infty}}{1 + B}. \quad (15)$$

Here $Y_{f,t}$ is the fuel mass fraction of the transferred material and is approximated as 1. This quantity accounts for any inert substances in the pyrolyzates. This assumes that $Le=1$, which means that the mass diffusivity equals the heat diffusivity. The mass fraction of fuel at the wall, $Y_{f,w}$, was obtained from mass and energy balances at the fuel surface:

$$\frac{QY_{o,\infty}/\nu_o M_o - h_w}{L} = B = \frac{Y_{f,w} + sY_{o,\infty}}{Y_{f,t} - Y_{f,w}} \quad (16)$$

Since $Y_{o,\infty}$, $Y_{f,t}$, s and B are all approximately constant and known for a given fuel, $Y_{f,w}$ and γ can be calculated as approximately constant for a given fuel material. For this study, B and γ are assumed to be 1.2 and 0.50 for wood firebrands (Woycheese 2000).

Disk and cylindrical firebrands – two limiting cases for combustion mass loss

The mass loss of disk and cylindrical firebrands in reality occurs through regression in both the radial and axial directions. To study the impact of the assumption of uniform regression in either of these directions, two limiting cases are studied: regression only in the axial direction, and regression only in the radial direction.

Since the gravitational, drag, and lift forces of a disk firebrand all linearly depend on radius, it cancels out of the force balance shown in equation (7). The relative velocity of a disk firebrand is therefore not a function of its radius. And similarly, thickness cancels out of the force balance on a cylindrical firebrand, so its relative velocity does not depend on length, as shown in equation (8). If C_N is assumed not to be strongly affected by the change in the h to r ratio for

these cases, drag and lift forces will remain at their initial, maximum level throughout the firebrand's flight. The radial regression of disk firebrands and axial regression of cylinder firebrands, then, are one extreme where regression has minimal effects on dynamics. The trajectories of these kinds of firebrands are similar to non-burning firebrands in Himoto and Tanaka (2005). On the other hand, combustion driven regression has maximum effect on dynamics for the other extremes of axial regression of disk firebrands or radial regression of cylindrical firebrands, since all regression occurs in the direction that does impact lift and drag forces. While the latter case appears to be more common, real firebrands may be expected to behave somewhere between these two extremes.

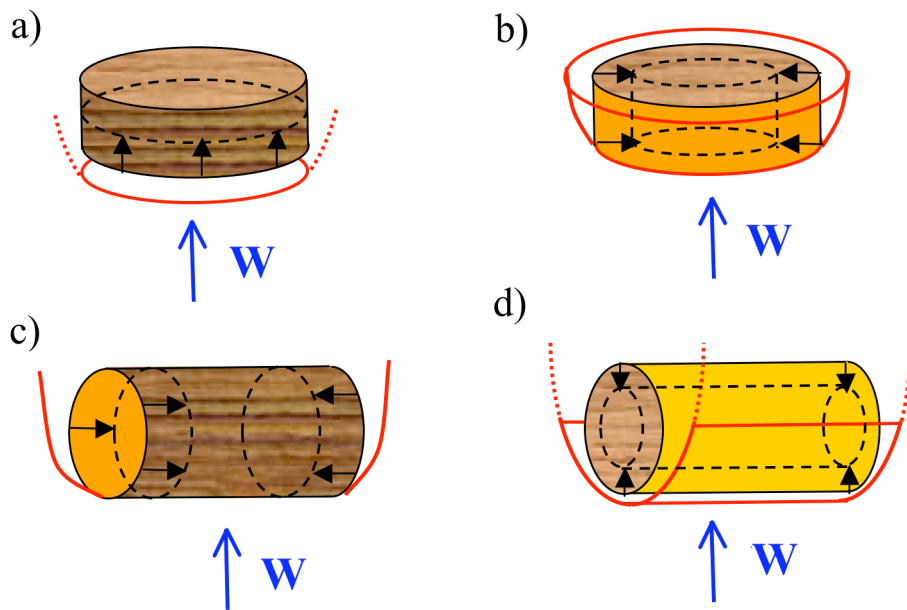


Figure 5. Four combustion models for disks and cylinders: a) a disk with axial regression (DSK_{dh/dt}), b) a disk with radial regression (DSK_{dr/dt}), c) a cylinder with axial regression (CYL_{dh/dt}), and d) a cylinder with radial regression (CYL_{dr/dt}). Red solid lines indicate the flame sheet in the boundary layer, and the red dotted line indicates possible flames that are ignored in the model. The black arrows indicate the regression direction, the black dotted lines indicate the shape of the firebrand after uniform regression, and the orange and yellow surfaces are the burning regions. For each of these cases, $\alpha = 90^\circ$.

The four combustion models are illustrated in Fig. 5. In the images in Fig. 5, the angle of attacks are set to 90° , the position of maximum drag. Boundary layer diffusion flames are formed around the burning surface in each case. A combusting stagnation-point boundary layer of uniform thickness is formed in the case of disk firebrands with axial regression, shown in Fig. 5a. Combusting boundary layers similar to the boundary layer for parallel flow over a flat plate

(Emmons 1956) are formed in the other three cases, shown in Figs. 5b, 5c, and 5d. As a first approximation, the combustion process is averaged over the burning surface so that the radius or length/thickness are uniformly regressed, and the firebrands retain their shape. Below, the various mass loss or mass regression models are described for the axial and radial regression of disks and cylinders. Figure 6 shows the dimensionless regression rates for the four combustion models, as a function of B , for use in future work. In this study, B is assumed to be 1.2 for wood.

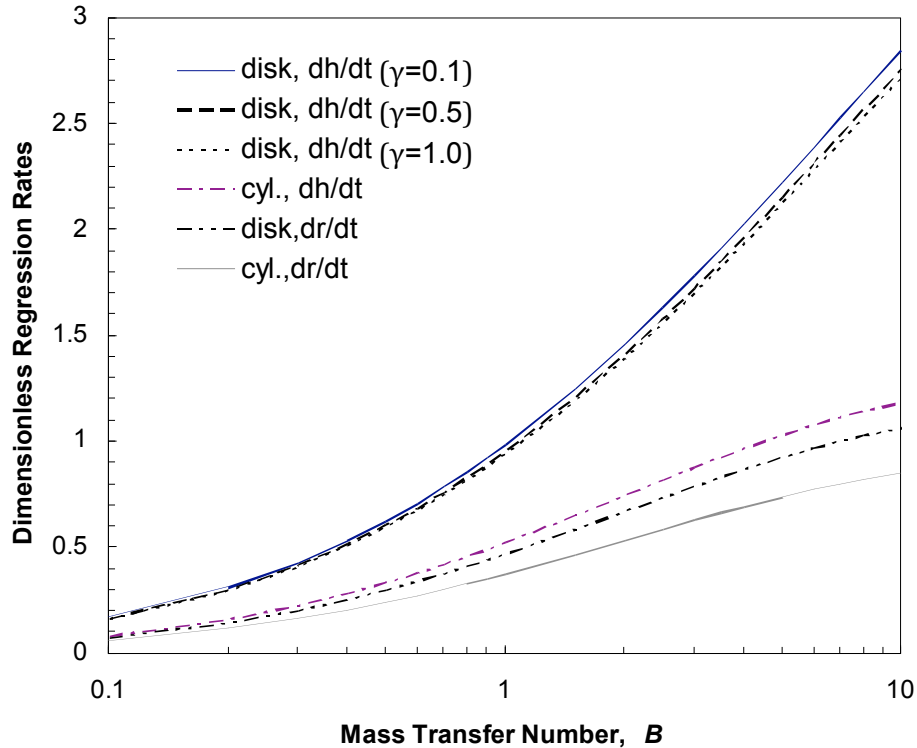


Figure 6. Dimensionless regression rates for the four combustion models shown as functions of the mass transfer number, B . Only the axial regression rate of the disk firebrand is a weak function of mass consumption number, γ , while others are independent of γ . Dimensionless regression rates are defined in equation (29).

4. Key findings

Using the firebrand model described in the previous section, copious simulations were performed. First, simulations with simplified fuel conditions and flat terrain using various models were performed to identify critical factors of firebrand transport phenomenon. After those simulations, simulations with realistic conditions were carried out. These studies show that the flame and plume structures are critical for firebrand simulations, and topography is

recognized as the significant factor in determining flame and plume structure. Simulations with various idealized topography are currently in progress.

A. Surface fire Simulations with flat terrain

The four models of firebrands with and without terminal velocity approximations are compared in the context of surface fire simulations. Disk and cylindrical models with limiting cases of combustion models were tested. The inlet boundary conditions are sheared-wind profiles using $U_x = 6(z/2.26)^{1/7}$ (one-seventh power law with 6 m s^{-1} at $z=2.26 \text{ m}$ above the ground), where mid-flame height is assumed. Table 1 shows a summary of the results from 8 surface fire simulations with various models and assumptions. The average initial size of effective firebrands are almost the same with the different models: 0.09 g disk with a thickness of 1.65 mm and 0.03 g cylinder with a diameter of 1.64 mm. Note that the sizes of the firebrands, which actually indicates the ability of the fire to loft them, are small since these are surface fires. In surface fires, the fuel bed is very close to the ground, and therefore the winds do not have much room to accelerate below the firebrands. As a result, the vertical velocities at the location where the firebrands are to be launched are fairly small ($\sim 7.5 \text{ m s}^{-1}$). However, the size of the launched firebrands in these simulations are comparable to some types of surface fuel, such as thin bark fragments for the disk model and pine needles for the cylindrical model.

Table 1. Summary of surface fire simulations with various firebrand models

Simulation With and without. Terminal velocity approximation (TVA)	Number of effective firebrands With TVA, (wo. TVA)	Average initial mass With TVA, (wo. TVA) (g)	Average travel distance With TVA, (wo. TVA) (m)	Average Flight time With TVA, (wo. TVA) (s)	Maximum. initial mass With TVA, (wo. TVA) (g)	Maximum travel distance With TVA, (wo. TVA) (m)	Maximum flight time With TVA, (wo. TVA) (s)
DSK_dh/dt w.TVA (wo. TVA)	33865 (34621)	0.09 (0.09)	1.7 (6.4)	1.27 (1.84)	0.13 (0.08)	41.0 (50.8)	15.34 (7.34)
DSK_dr/dt w.TVA (wo. TVA)	31762 (32667)	0.09 (0.09)	1.3 (6.60)	1.05 (1.80)	0.06 (0.14)	10.7 (227.80)	6.66 (26.36)
CYL_dh/dt w.TVA (wo. TVA)	14300 (15783)	0.003 (0.003)	1.07 (1.79)	0.86 (7.30)	0.003 (0.002)	9.30 (82.30)	2.60 (9.58)
CYL_dr/dt w.TVA (wo. TVA)	16151 (14580)	0.003 (0.003)	1.27 (7.4)	0.95 (1.77)	0.003 (0.003)	11.8 (26.4)	5.26 (3.30)

As shown in Table 1, the models without the terminal velocity assumption are found to travel further because removing the assumption allows the momentum of the firebrands to carry their speed beyond the point where the winds slow down. Remember that with the terminal velocity approximation the horizontal velocity will always be equal to the wind at that location since there is no horizontal body force. In reality and without the terminal velocity approximation, firebrands can fly faster than their immediate surrounding winds if they carry momentum from stronger winds that they were previously exposed to. This is essentially the notion of a firebrand being thrown by locally strong winds, whereas with the terminal velocity approximation firebrands can not be thrown, because it is similar to throwing a piece of dust. The average travel distances are 1.07 m to 1.7 m with the terminal velocity assumption and 6.4 m to 7.4 m without terminal velocity.

As described in the models section, the shape change of firebrands due to combustion can affect the aerodynamics of the firebrand. Combustion affects the trajectories of DSK_dh/dt and CYL_dr/dt, not DSK_dr/dt and CYL_dh/dt. The combustion effects made DSK_dh/dt and CYL_dr/dt travel farther with the terminal velocity assumption. However, the momentum of firebrands is much more significant than the combustion effect on trajectories. Since DSK_dr/dt and CYL_dh/dt have a smaller burning area, they have a longer lifetime, and it is also possible for them to have larger travel distances. In the cases of DSK_dh/dt and CYL_dr/dt, the firebrands tend to burn faster and burnout more easily since the area burning is a more significant amount of the surface area, and so they have shorter travel distances. Figure 7 shows scatter plots of travel distance versus initial mass, in which each dot represents an effective firebrand. As shown in Fig. 7, eliminating the terminal velocity assumption, which is more realistic with dynamic wind fields, allows circumstances where firebrands can be carried farther. Figure 8 shows the launching and landing positions of 500 firebrands that traveled farthest for each model. The initial fire line is at $x = -220$ m, and is 100 m long. Figure 10 shows how the fire line spreads over 40 second intervals (Fig. 9-a) at 40 s, Fig. 9-b) at 80 s, Fig. 9-c) at 120 s, and Fig. 9-d) at 160 s). As observed in wind-driven surface fire experiments (Anderson 1983; Fons 1946), the fastest spread in the axial direction occurs at the center of the fire line, which takes on a relatively symmetric crescent shape. Detailed discussions about the shape of the fire line in surface fires is presented in Linn and Cunningham (2005).

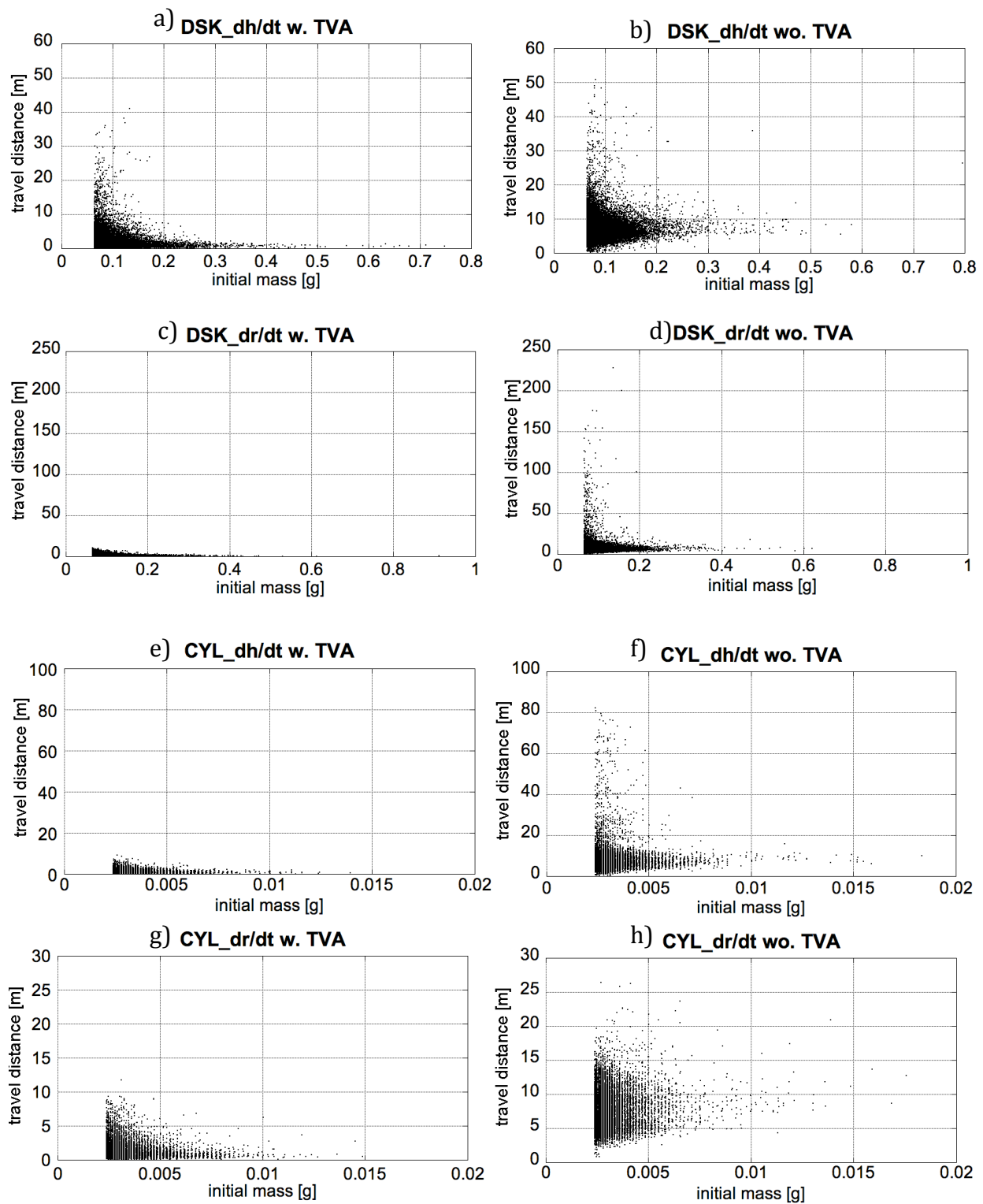


Figure 7. Travel distance versus initial mass of various firebrand models in surface fire simulation with 6m/s wind at the mid-flame height: a) DSK_dh/dt w. TVA, b) DSK_dh/d wo. TVA, c) DSK_dr/dt w. TVA, d) DSK_dr/d wo. TVA, e) CYL_dh/dt w. TVA, f) CYL_dh/d wo. TVA, g) CYL_dr/dt w. TVA, and h) CYL_dr/d wo. TVA.

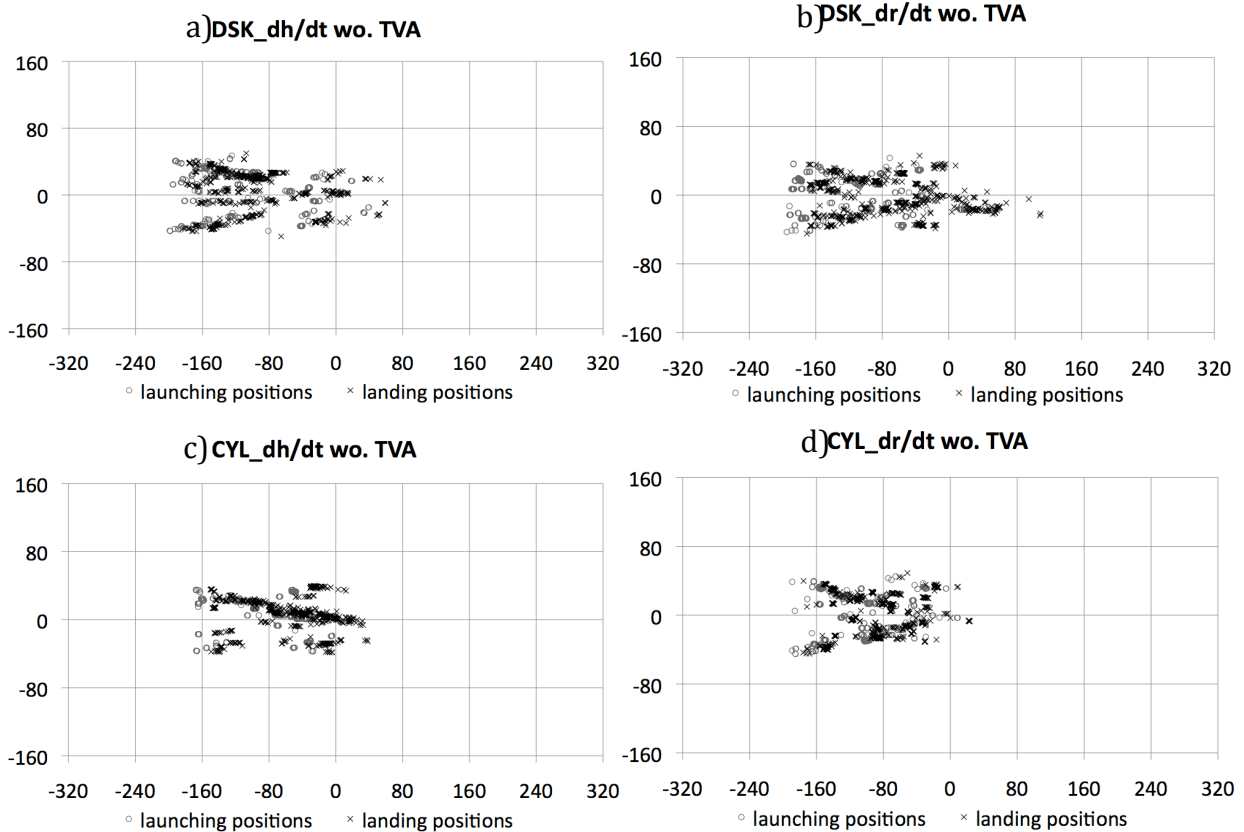


Figure 8. Launching positions (grey circles) and landing positions (black crosses) of 500 firebrands with the furthest travel distance for various models without terminal velocity assumption in surface fire simulations with a 6 m s^{-1} wind at mid flame height: a) DSK_dh/dt wo. TVA, b) DSK_dr/dt wo. TVA, c) CYL_dh/dt wo. TVA, and d) CYL_dr/dt wo. TVA.

The launching and landing locations of the firebrands with longer travel distances are directly related to the buoyant plume structure. It is observed in Fig. 8 that the firebrands having the longest trajectories come from particular regions near the edges and in the center of the fire line. This trend is illustrated by the fact that there is not an even distribution of grey circles in the burned region and the streaks of launching/landing positions in Fig. 8. The locations of concentrated firebrand launches resulting in long trajectories in the interior of the fire line varies from simulation to simulation. However, in each of the simulations the combined buoyant force and vertical vortices that occur near the ends of the fireline cause focal points for long traveling firebrands. As the firelines progress and the shape of the lines become more curved, the center of the fireline, or the apex of the curved fire shape, becomes a focal point for launching firebrands that will travel long distances. These regions of strong buoyant plume are shown in Fig. 9. Further discussion on the effects of plume structure on firebrand transport, which determines

launching/landing positions of long-distance firebrands, is presented in the canopy fire simulation section below.

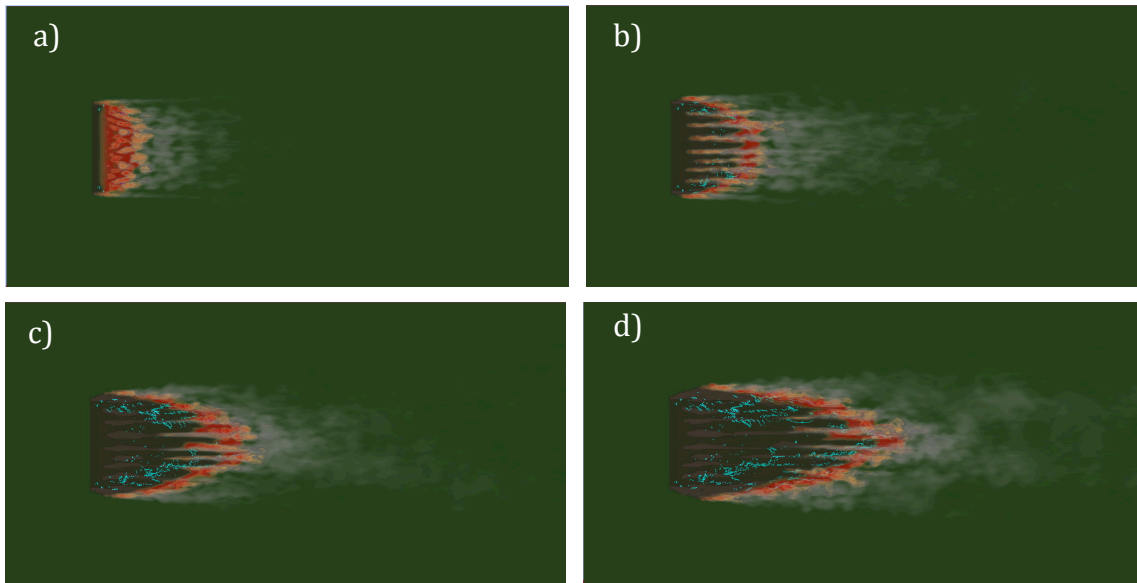


Figure 9. Top view of surface fire simulations with CYL_dr/dt models as the fire progresses. The first picture shows 40 seconds after ignition and time between each frame is 40 seconds: a) 40 seconds, b) 80 seconds, c) 120 seconds, and d) 160 seconds after ignition. Turquoise dots indicate where effective firebrands have landed.

B. Crown fire simulations with flat terrain

The disk and cylindrical firebrand models are simulated in the context of a fire burning in both canopy and surface fuels. Firebrands are modeled without the terminal velocity assumption, since it has been shown that the terminal velocity assumption is not valid with dynamic wind fields from HIGRAD/FIRETEC simulations. The same wind shear profile used in the surface fuel simulations is used as a boundary condition for the crown fire simulations; however, the drag from the canopy modifies the wind profile during the simulation. The effects of drag from the canopy on wind shear profiles when using HIGRAD/FIRETEC has been discussed in Pimont *et al.* (2009). The wind speed at the boundary is approximately 9.3 m s^{-1} at 50 m from the ground.

Table 2 shows a summary of the results from four firebrand simulations with the crown fire scenario. Crown fires definitely have a greater ability to launch firebrands than surface fires: the fire in the deeper fuel bed induces stronger buoyant forces, and there is more space below the

canopy for winds to accelerate upward to the point where the firebrands are launched. Thus, larger numbers of substantial sized firebrands are launched from crown fires and transported significant distances. By comparing Table 1 and Table 2, it can be seen that the discrepancy between the number of effective disk firebrands and cylindrical firebrands is larger in the crown fire simulations than for the surface fire simulations. This is because disks are more aerodynamically responsive to local winds than cylinders due to the disk's larger drag and the crown fires have stronger buoyant plume structure, which contains a wide distribution of vertical velocities.

Remember that the disk firebrands represent thin flat firebrands such as those caused by bark flakes or even those produced by building materials. The firebrands from grasses, twigs or needles should have cylindrical shapes, as observed in recent experiments (Manzello *et al.* 2007). The combustion model that is the most realistic for firebrands from forest fires, which would be broken pieces of tree needles, twigs and branches, should be the radial direction cylinder regression model (CYL_dr/dt). The high numbers of effective disk firebrands with significant thicknesses shown in Table 2 indicate that structures in wildland/urban intermix (WUI) areas could be sources of the more dangerous firebrands. The study of structure fires as a firebrand source should be carried out together with a study of structures as a recipient fuel for firebrands.

Table 2. Summary of crown fire simulation with various firebrand models

Simulation With and without. Terminal velocity approximation (TVA)	Number of effective firebrands without. TVA	Average initial mass without. TVA TVA, (g) (Thickness or radius (mm))	Average travel distance without. TVA (m)	Average Flight time without. TVA (s)	Maximum. initial mass without. TVA (g) (Thickness or radius (mm))	Maximum travel distance without. TVA (m)	Maximum flight time without. TVA (s)
DSK_dh/dt, wo. TVA	157343	5.40 (6.32)	73.4	13.71	11.85 (8.03)	502.4	49.14
DSK_dr/dt, wo. TVA	205304	5.01 (6.20)	91.21	14.36	2.46 (5.05)	530.21	54.58
CYL_dh/dt, wo. TVA	8335	0.41 (4.15)	88.16	13.42	0.41 (4.16)	516.26	45.28
CYL_dr/dt, wo. TVA	4813	0.43 (4.21)	60.66	11.20	1.88 (6.93)	300.01	33.22

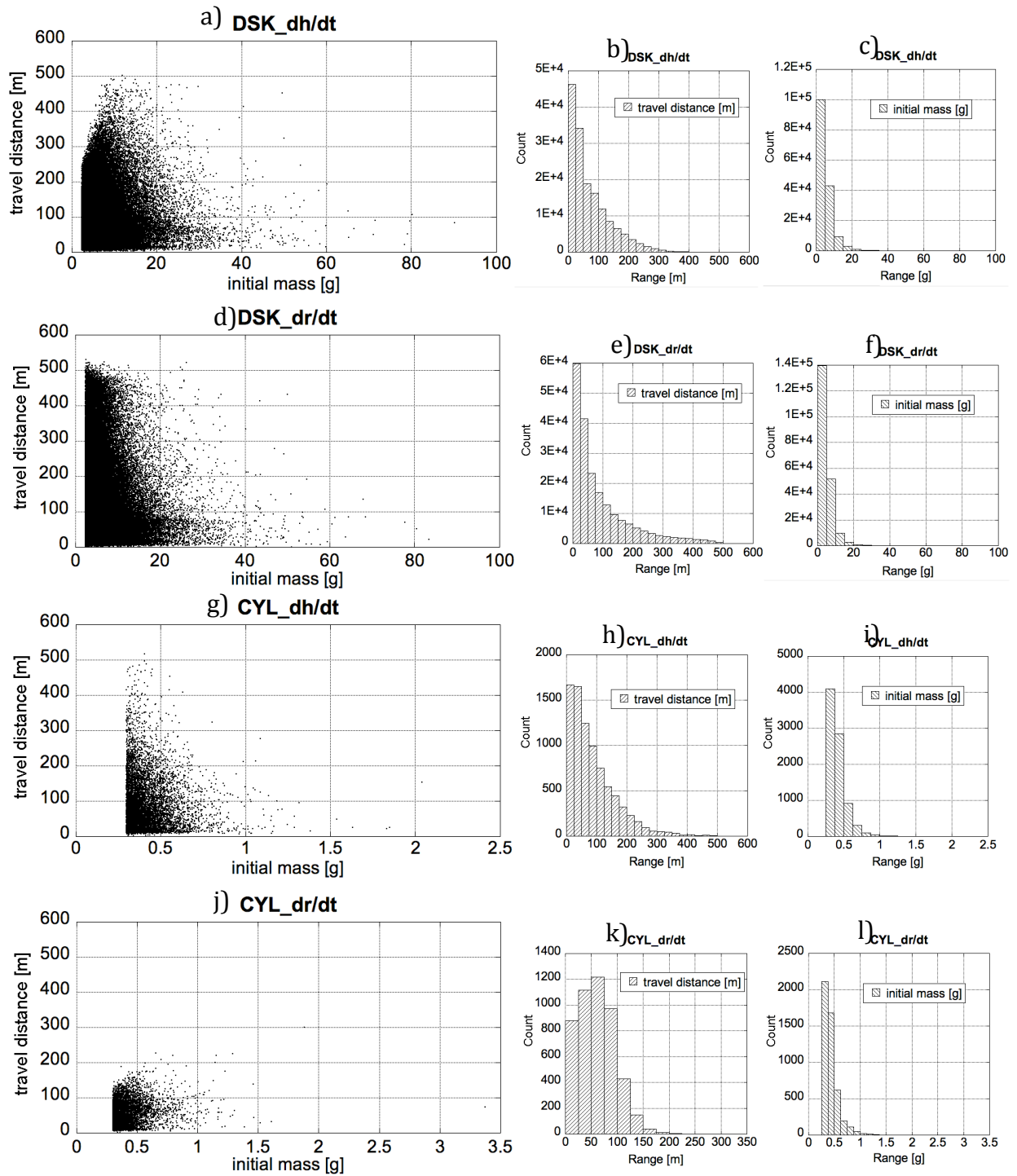


Figure 10. Travel distance versus initial mass of various firebrand models without terminal velocity assumption in canopy fire simulation: DSK_dh/dt - a) scatter plot, b) histogram of travel distance, and c) histogram of initial mass; DSK_dr/dt - d) scatter plot, e) histogram of travel distance, and f) histogram of initial mass; CYL_dh/dt - g) scatter plot, h) histogram of travel distance, and i) histogram of initial mass; CYL_dr/dt - j) scatter plot, k) histogram of travel distance, and l) histogram of initial mass.

Figure 10 shows traveled distance and initial mass of firebrands in the crown fire simulations with scatter plots and histograms. Note that the number of effective firebrands indicates the relative potential of firebrand transport for each case, rather than the numbers of actual

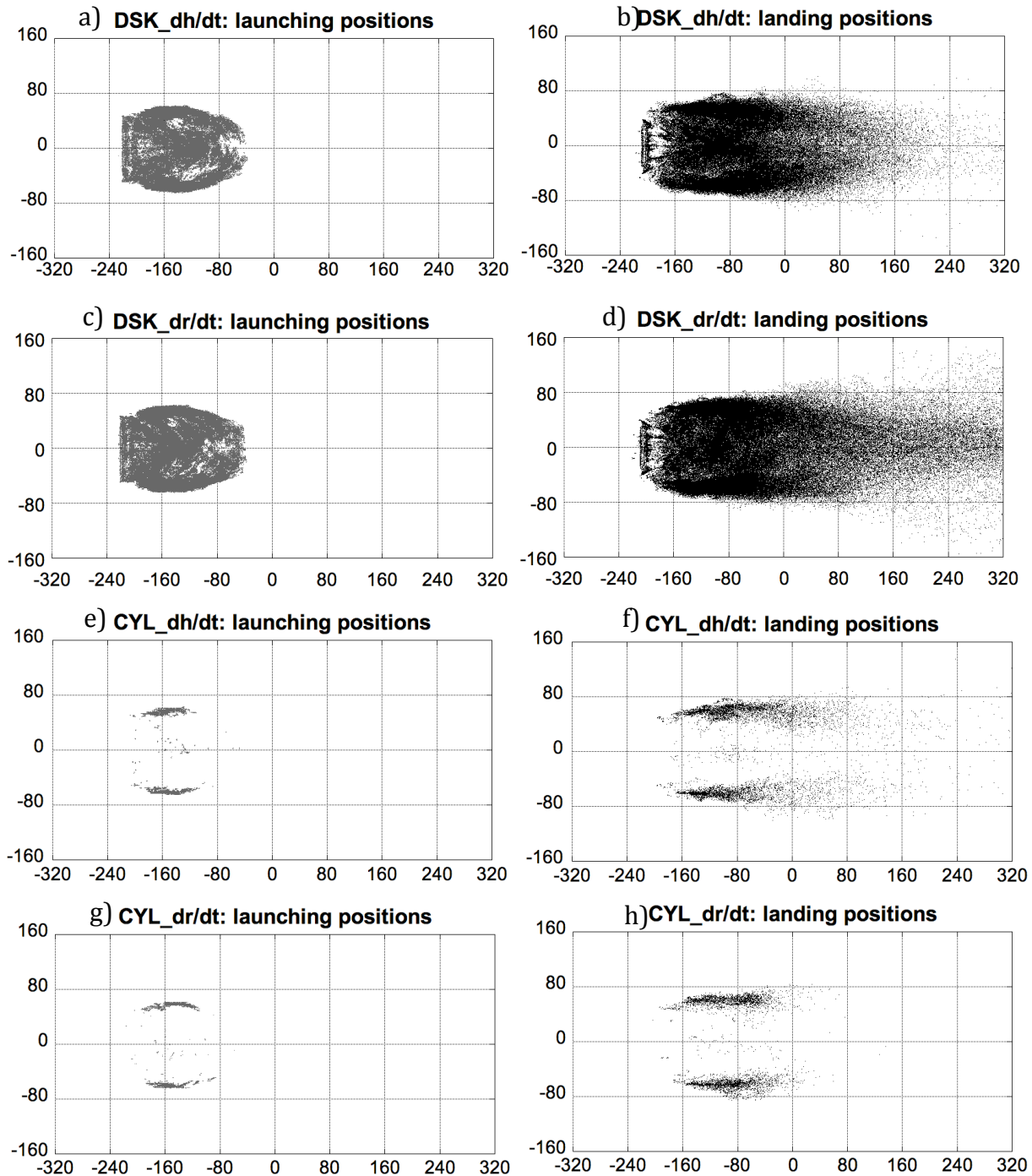


Figure 11. Launching positions (grey dots in a), c), e), and g)) and landing positions (black dots in b), d), f), and h)) of firebrands in crown fire simulations: DSK_dh/dt - a) launching positions, b) landing positions; DSK_dr/dt - c) launching positions, d) landing positions; CYL_dh/dt - e) launching positions, f) landing positions; CYL_dr/dt - g) launching positions, h) landing positions.

firebrands that could be produced in each scenario. In the cases where combustion mass loss does not affect the aerodynamics of firebrands, DSK_dr/dt and CYL_dh/dt , the most probable travel distance is near zero and the maximum travel distance occurs for brands with minimal mass. The limiting cases where combustion models affect aerodynamics the most, DSK_dh/dt and CYL_dr/dt , have maximum travel distances arriving that are shorter than DSK_dr/dt and CYL_dh/dt respectively, but these maximum travel distances occur for firebrands of larger mass than the minimum. These trends are caused by the increase in surface area/weight ratios that occur simultaneously as the firebrands burn at a faster rate than the DSK_dr/dt and CYL_dh/dt cases. The smallest firebrands in DSK_dh/dt and CYL_dr/dt burn out before they land. This is also related to the lower numbers of effective firebrands in $DISK_dh/dt$ and CYL_dr/dt than in $DISK_dr/dt$ and CYL_dh/dt in Table 2.

Figure 11 shows scatter plots of firebrand launching and landing positions. Each dot represents an effective firebrand in the simulations. As discussed for surface fire simulations, plume structure determines where dangerous firebrands are launched and land. Similar to the surface line fire behavior, strong buoyant vortices develop at the edge of the firelines in all of the simulations. For cylinder simulations, most of the firebrands are launched at the edges, with a few effective firebrands launched at the center of the fireline. During 170 seconds of simulated fire spread, the buoyant vortex aided by entrainment at the edge is stronger than at the center of the fireline. Thus, cylindrical firebrands, which are not as aerodynamically favored as disks, are

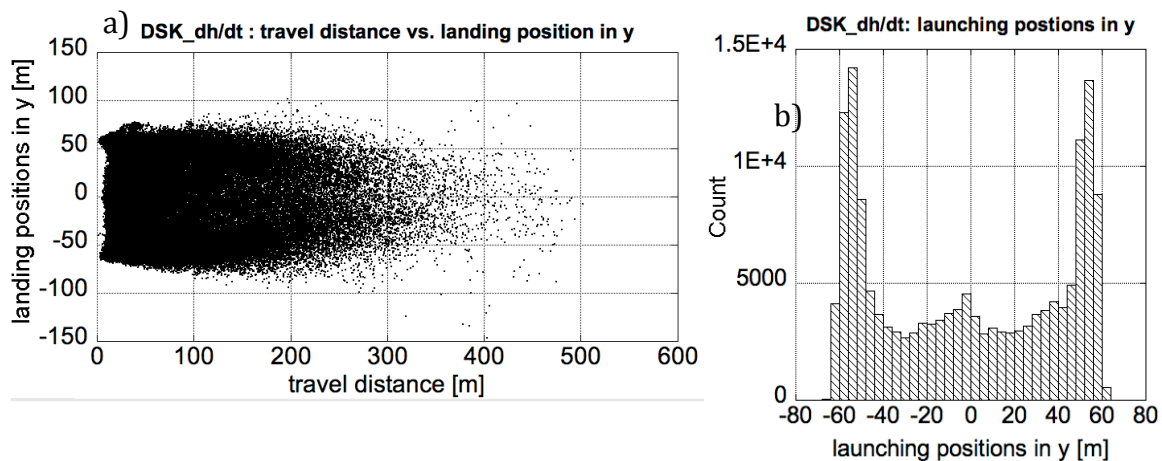


Figure 12. a) Travel distance versus landing positions in the y-direction: firebrands that traveled further landed near the centerline of the fireline. b) Firebrand launching distributions in the y-direction: the edges of the fireline launched more firebrands.

picked up at the edges but infrequently in the center. For disk firebrands, which are more easily lofted, launch sites are more distributed throughout the moving fire perimeter. The buoyant updrafts in the interior of the fire include stronger vertical winds above the canopy than they did for surface fuels, and so they are more effective at picking up the disk firebrands throughout the fireline. The disk firebrands, which are lofted higher than cylinders, are trapped deeper within the large buoyant plume and stay longer near the centerline of the plume. Thus, firebrands with longer travel distances primarily land near the centerline of the domain, as shown in Fig. 12a. Figure 12 shows a scatter plot of travel distance versus y-direction landing positions and a histogram of the y-direction launching positions from the DSK_dh/dt simulation. Though a higher percentage of the firebrands are launched near the edges of the fireline, as shown in Fig. 12b, those not trapped in the center of the plume tend to be ejected from the plume earlier in their trajectory, and therefore do not travel as far. At the edges, entrainment dilutes the hot gases with cooler air so buoyant forces are damped, while hot gases are drawn toward the center of the fireline to form the most concentrated area of the buoyant plume at the center of the burning region. If disks are trapped in the central area of the fireline, they can be carried higher than in

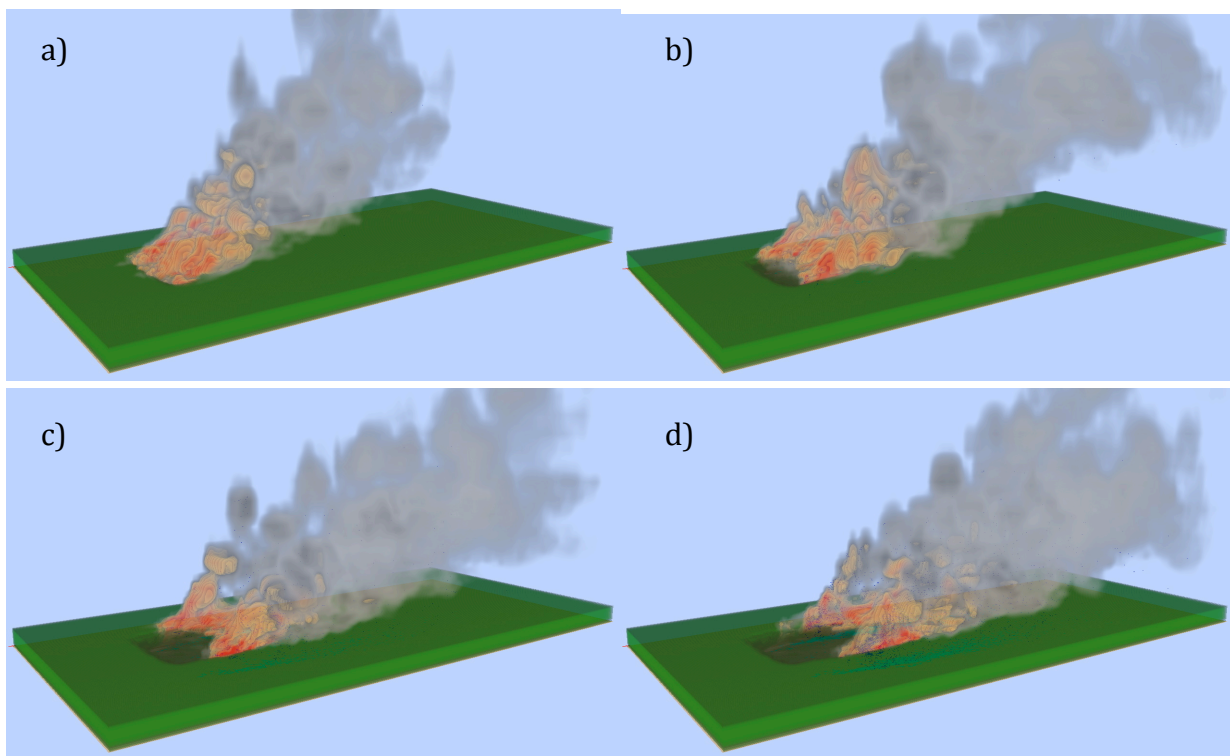


Figure 13. Crown fire simulation with CYL_dr/dt with the view from behind as fire progress. The first picture shows 40 seconds after ignition and time between each frame is 40 seconds: a) 40 seconds, b) 80 seconds, c) 120 seconds, and d) 160 seconds. Turquoise dots on the ground indicate where effective firebrands are landed.

the vortices at the edges. Visualizations of plume structure are shown in Fig. 13a at 40 s, Fig. 13b at 80 s, Fig. 13c at 120 s, and Fig. 13d at 160 s after ignition. At 120 seconds after ignition, shown in Fig. 13c, the strong vertical structure at the edges was already formed. The study of plume structure is crucial for the prediction of firebrand transport, which could lead to the prediction of potential spot ignition positions. The majority of previous studies of firebrand transport focused on maximum spot fire distance, however information about locations with a high probability of spot ignition are also important. For example, firebrands launched at the edge of the fireline could move laterally, as shown in Fig. 11, to initiate or assist the spread of flanking fires. Spotting near the edge of a fireline could cause the escape of a prescribed burn or fire in other wildfire management scenarios.

C. Las Vegas, NM, ICFME, and Angel Fire, NM

After completing simulations on flat terrain, simulations with real topography and fuels were performed. Figure 6 shows firebrand transport simulations for a hypothetical fire with three firelines. In order to show flying firebrands (dark blue) and firebrands landed on unburned fuel (light blue), flames and fuels are not visualized in Fig. 6. For this simulation, real fuels

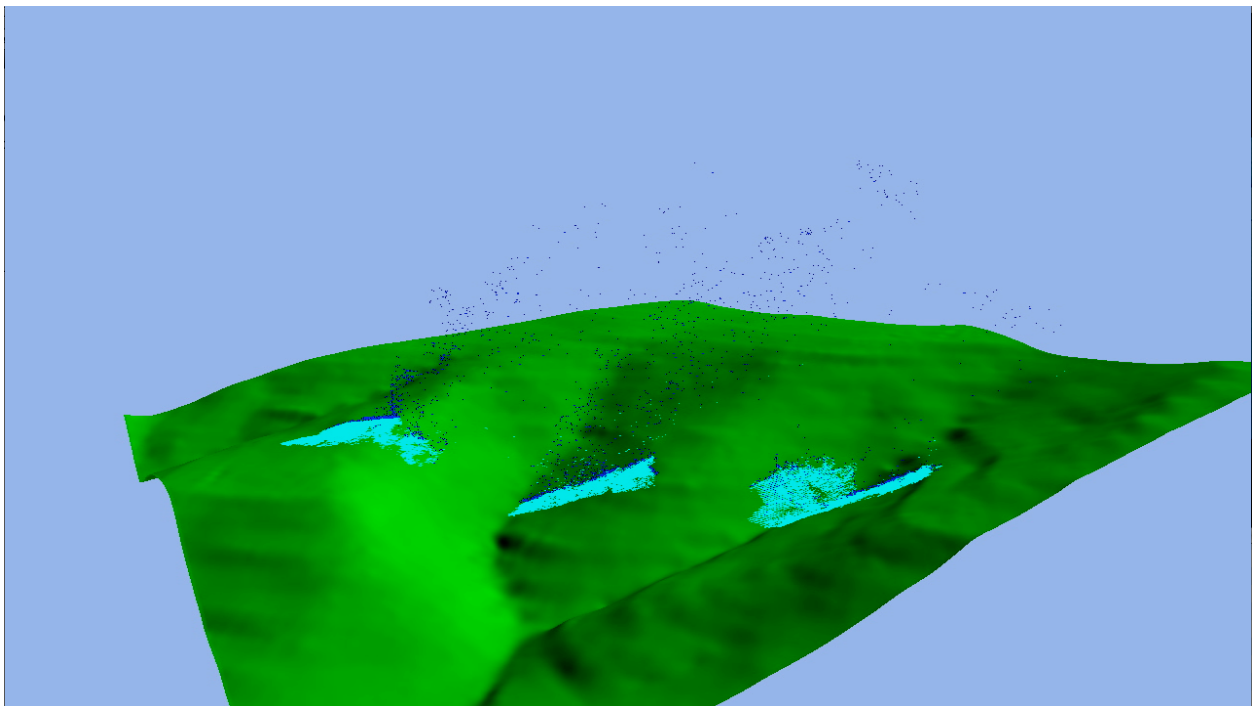


Figure 6. Illustration of firebrand transport in a HIGRAD/FIRETEC-SPOT simulation of hypothetical fires near Las Vegas, NM. In this image the forest fuels and fires have been removed to enable depiction of the launched and landed firebrands at this instant. Firebrands are emitted from three different fires with the dark blue dots being firebrands that are currently in flight and the light blue dots being firebrands that have already landed before burnout on unburned fuel.

determined from satellite images and historical RUC (Rapid Update Cycle) wind data were used. In this simulation, the topography and dynamic wind conditions, interacting with the plume structure that evolves as the fires grow, are found to play a critical role in firebrand behavior.

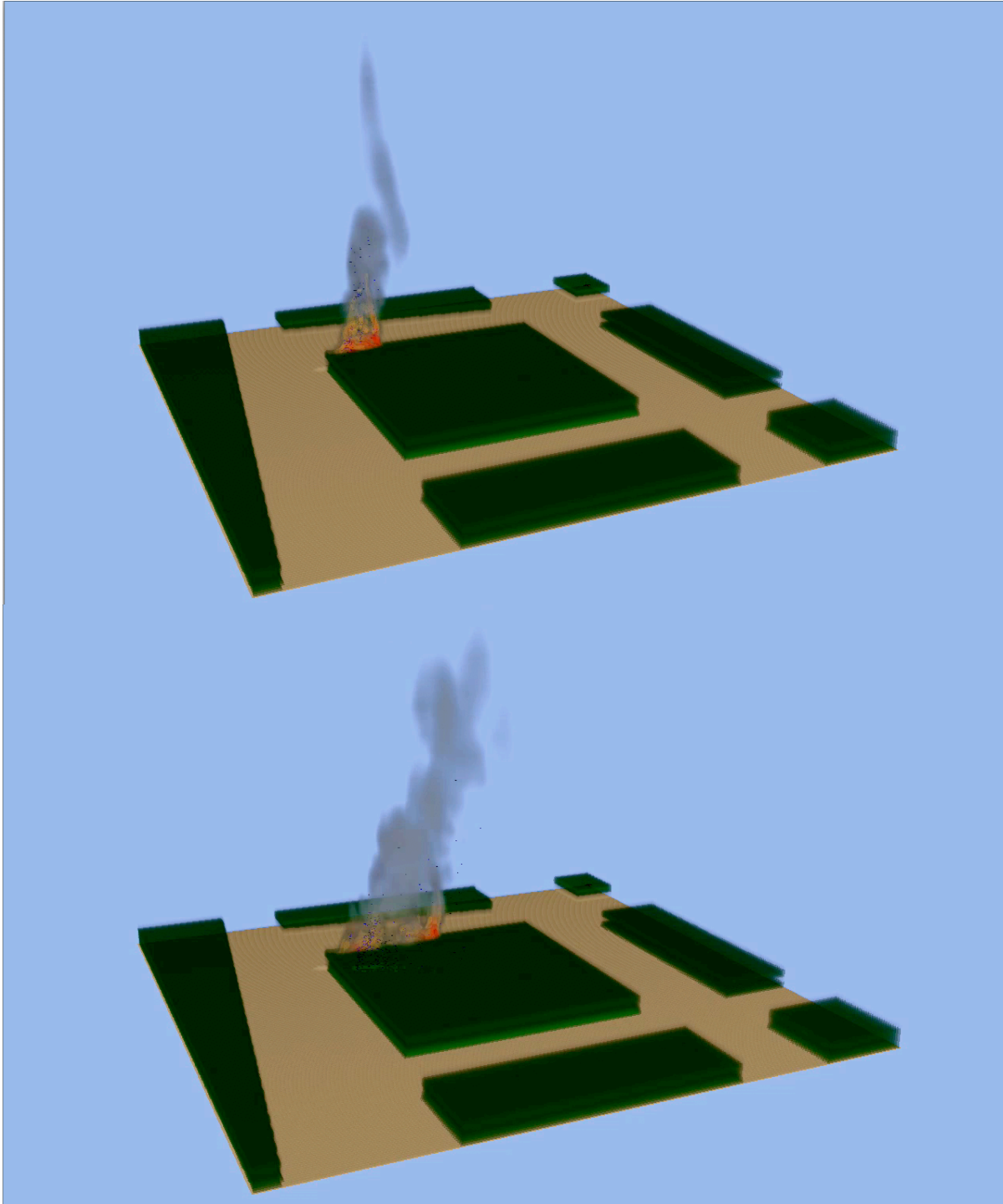


Figure 7. Firebrand simulations with ICFME (International Crown Fire Modeling Experiment) winds and fuels.

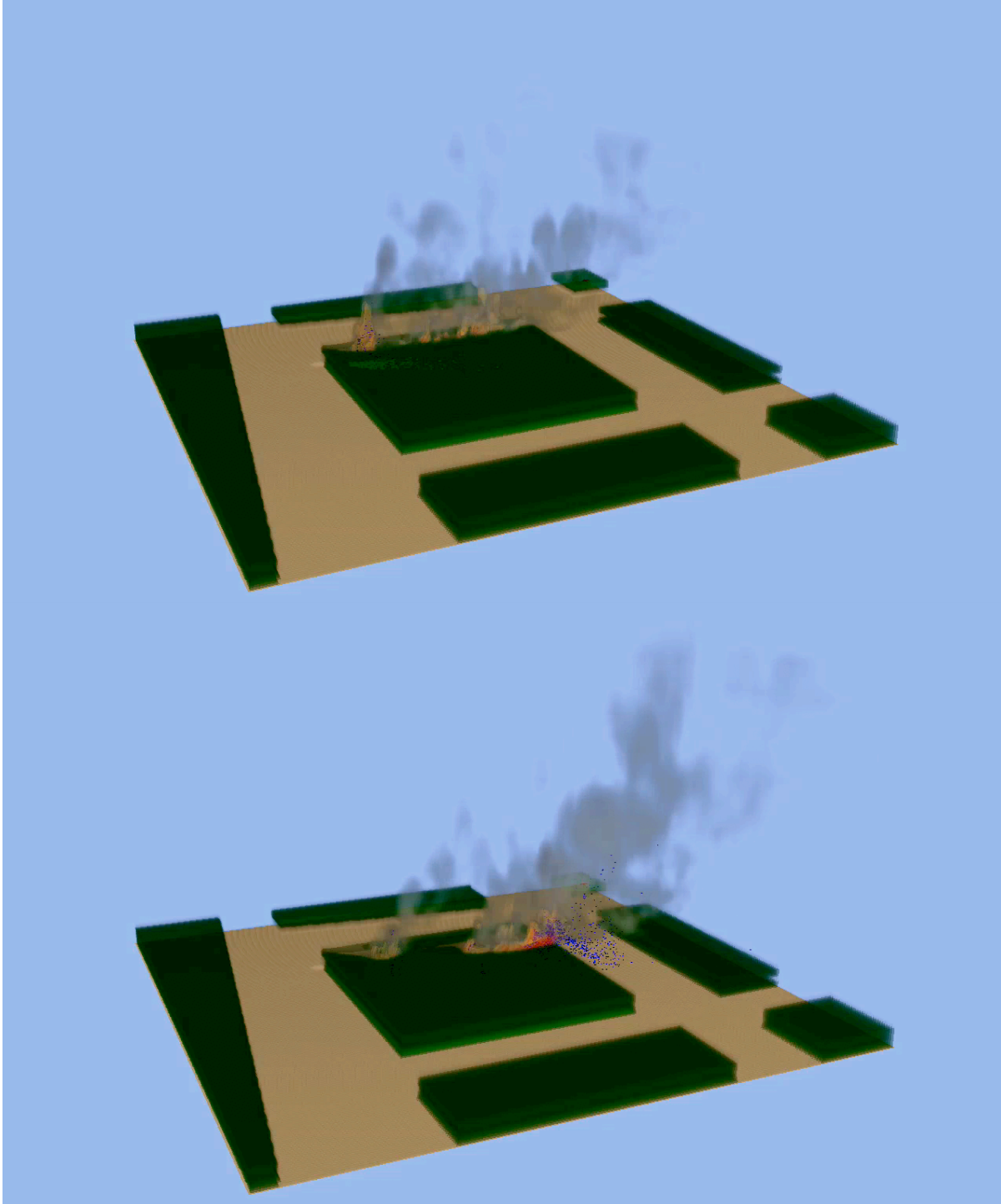


Figure 7. (cont.) Firebrand simulations with ICFME (International Crown Fire Modeling Experiment) winds and fuels.

Figure 7 shows firebrand simulations using ICFME (International Crown Fire Modeling Experiment) fuels and dynamic tower wind data. There were no significant spot fires observed

in the real experiments, and simulated firebrands all landed either within the ICFME plot being burned or in the neighboring fuel breaks. It is observed in the simulations that the firebrand launching and transporting behaviors are directly related to the dynamics of the ambient wind and the evolution of flames in the fireline.

Firebrand simulations were performed for another hypothetical fire set in Angel Fire, NM, where fuel-thinning strategies were being studied. Simulations were performed at one location with steep topography for both the unthinned and thinned fuel scenarios using historical winds from June 23, 2008. The position of the fire 60 s after ignition in the simulation using unthinned fuels was chosen to initiate the firebrand analysis. A time when the fire was at approximately the same position in the thinned simulation, 45 s after ignition, was used to initiate the spotting analysis in this simulation. In both simulations, firebrands were produced with the same generation rate and tracked for 25 seconds in order to compare the quantities and sizes of firebrands that were launched and their trajectories. Five firebrands are generated every second from each computational cell that has enough burning fuel. In both simulations, each computational cell covers a 2 m x 2 m area.

Figure 8 shows an image of the firebrand simulation for the thinned fuels case visualized with fuels and flame. Figure 9 shows snapshots of firebrand simulations in which dark blue dots are firebrands that are flying, and light blue dots are landed on unburned fuel, without fuel and flame visualized for better view. There are 137382 firebrands flying and 296746 firebrands landed in unthinned forest fires and 54719 firebrands flying and 24628 firebrand landed in thinned forest fires in these snapshots, which show 25 seconds of firebrand activity. Figure 10 shows images from these two simulations describing the launch and landing patterns of these fires. One issue that is apparent from this figure is that there are many more firebrands launched from the unthinned forest than the thinned forest during this 25 second time frame, 296746 and 24628 respectively. Obviously, both of these simulations suggest large numbers of firebrands being launched, however large fractions of these firebrands are landing close to the fireline and the fire overruns them before they even begin to develop into sizable fires. These short-distance firebrands can be of significant consequences to structures in wildland/urban interface, but it is still a matter of probabilities and the more firebrands that are launched, the more risk of them

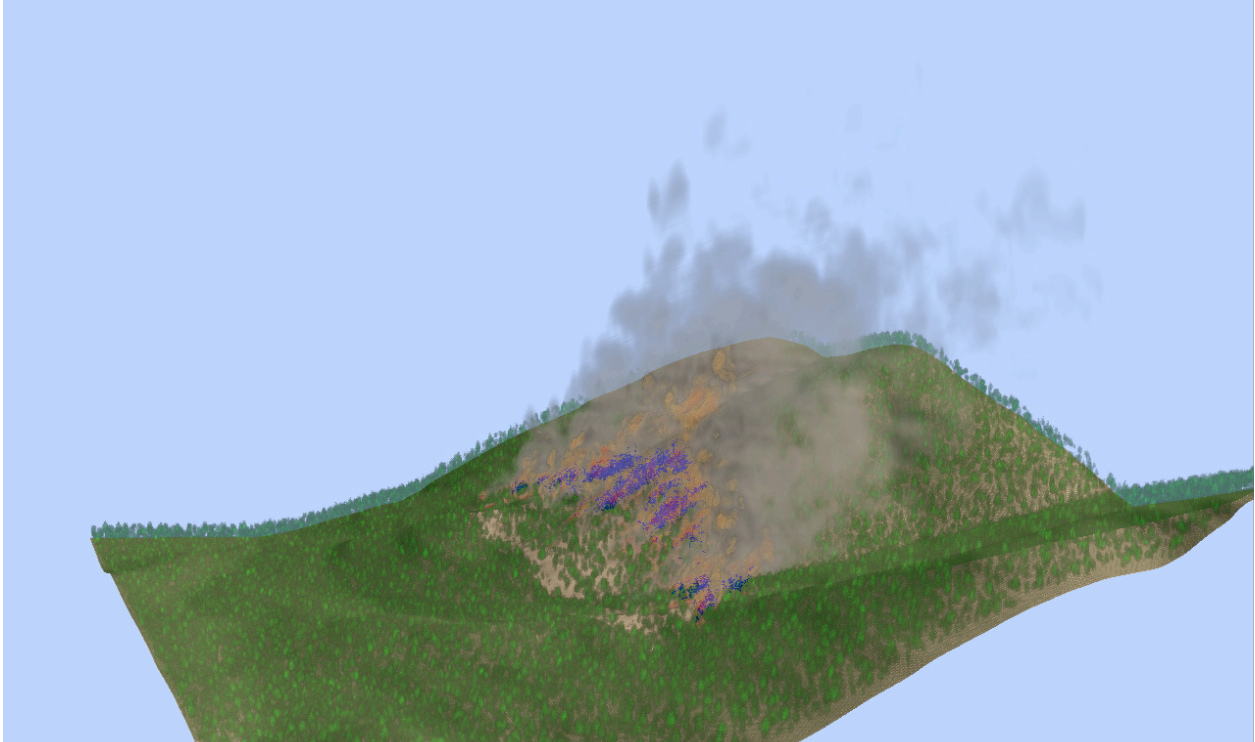


Figure 8. An image of the firebrand simulation for the thinned fuels scenario in Angel Fire, NM.

landing in vulnerable locations such as under shingles, under eaves, in air vents, etc. The impact of the longer traveling firebrands is also increased with the number of firebrands due to the fact that only a small fraction of these firebrands land in conditions which are conducive to ignition of new fires. Higher numbers of firebrand increase the probability of successful ignition of new fires at larger distances from the original head fire. Figure 10 includes plots that illustrate the numbers of firebrands of each size. Topography affects the launching and transport processes of firebrands and the distance that these firebrands travel is expected to be larger in if the simulated fires were approaching a ridge or saddle. Figure 11 illustrates the launched and landing locations of the 500 firebrands that traveled the farthest in each simulation. Clearly their potential of having long distance spotting is higher in the unthinned forest simulations. The maximum distance for firebrands in the unthinned forest simulation is 291 m whereas it is 130 m for the thinned forest simulation. It is also observed that the lateral distribution of these long-range firebrands in the unthinned forest is wider than thinned forest fire. This implies that firebrand activity in the unthinned forest may contribute more to fire spread in the wider range of fireline than long-range firebrands in the thinned forest, which seems to be limited at the center of the fireline. These images of firebrand launching and landing only capture firebrands launched and

landed in 25 seconds. The entire set of firebrands that are launched over the course of the fires creates a very crowded plot that is hard to decipher, and yet by visualizing this smaller set of

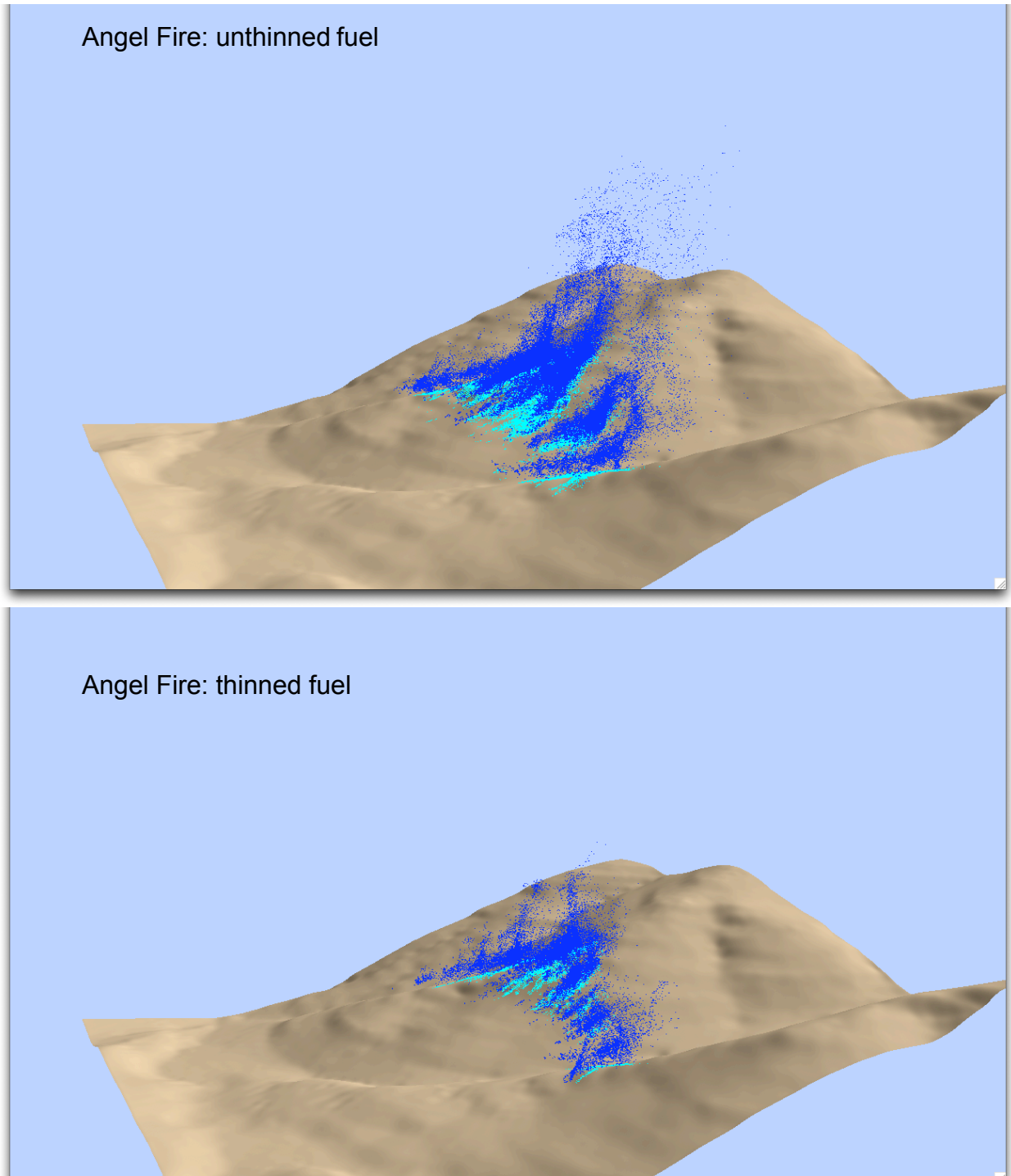


Figure 9. Illustration of firebrand transport in a FIRETEC simulation of hypothetical fires in Angel Fire, NM. In this image the forest fuels and fires have been removed to enable depiction of the launched and landed firebrands at this instant. Above: In the unthinned forest case, there are 137382 firebrands flying (dark blue dots) and 296746 firebrands landed (light blue dots). Below: In the thinned forest case, there are 54719 firebrands flying (dark blue dots) and 24628 firebrands landed (light blue dots).

firebrands the differences in the spotting behavior can be seen. The higher intensity fire in the unthinned forest results in more prevalent and longer distance spotting. The other impact of the fuel structure is the fact that the stronger plume in the unthinned forest blocks out the ambient wind and so allows the firebrands to have a stronger initial vertical motion. This stronger vertical motion lifts larger firebrands as well, as shown in Fig. 10.

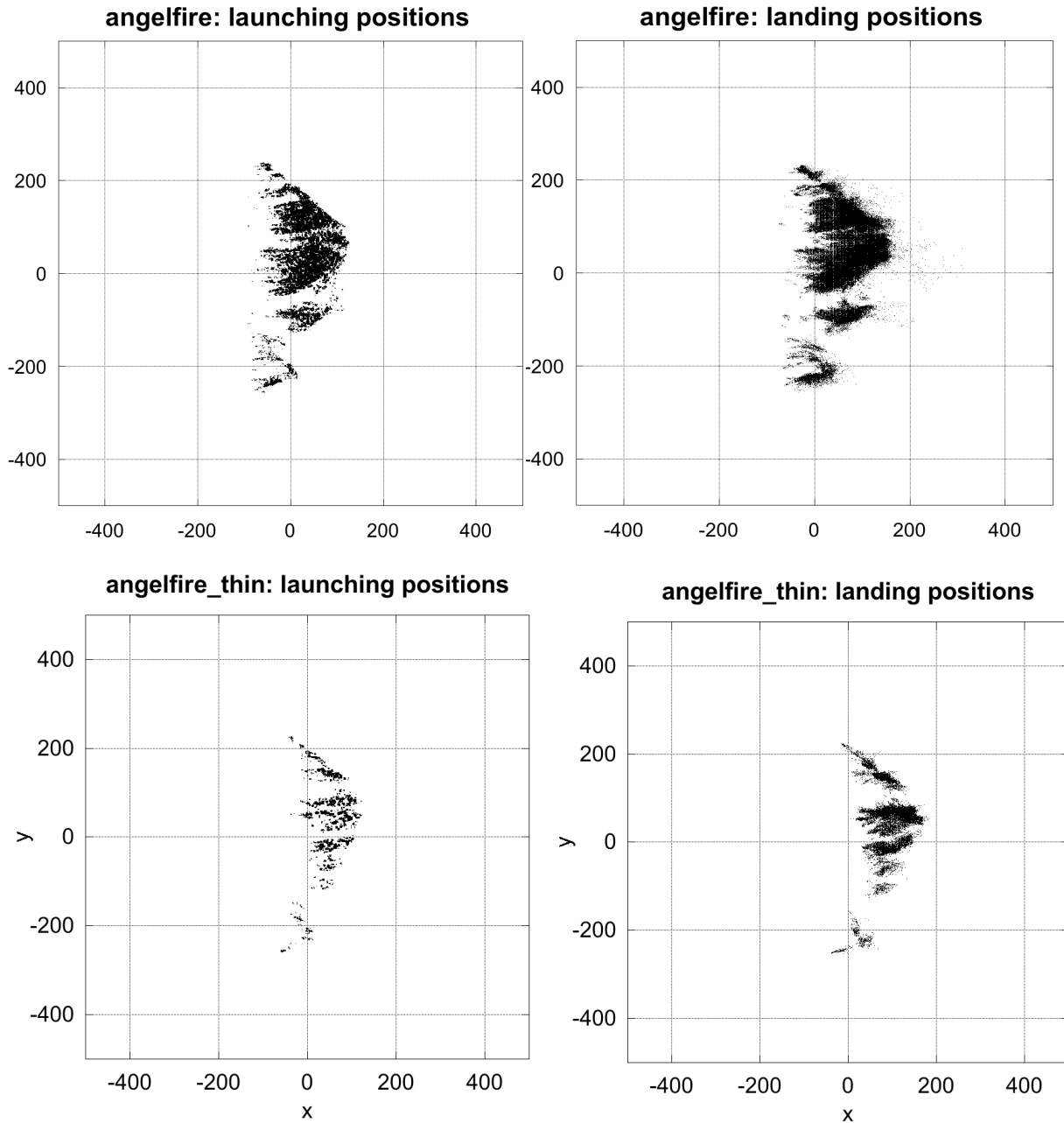


Figure 10. Diagrams of the positions and densities of launching and landing positions of firebrands during the selected 25 s. period for the thinned and unthinned forest simulations with winds from June 23, 2008. Close observation of the “angelfire: landing positions plot” reveals numerous firebrands landing up to 100 m past the main population.

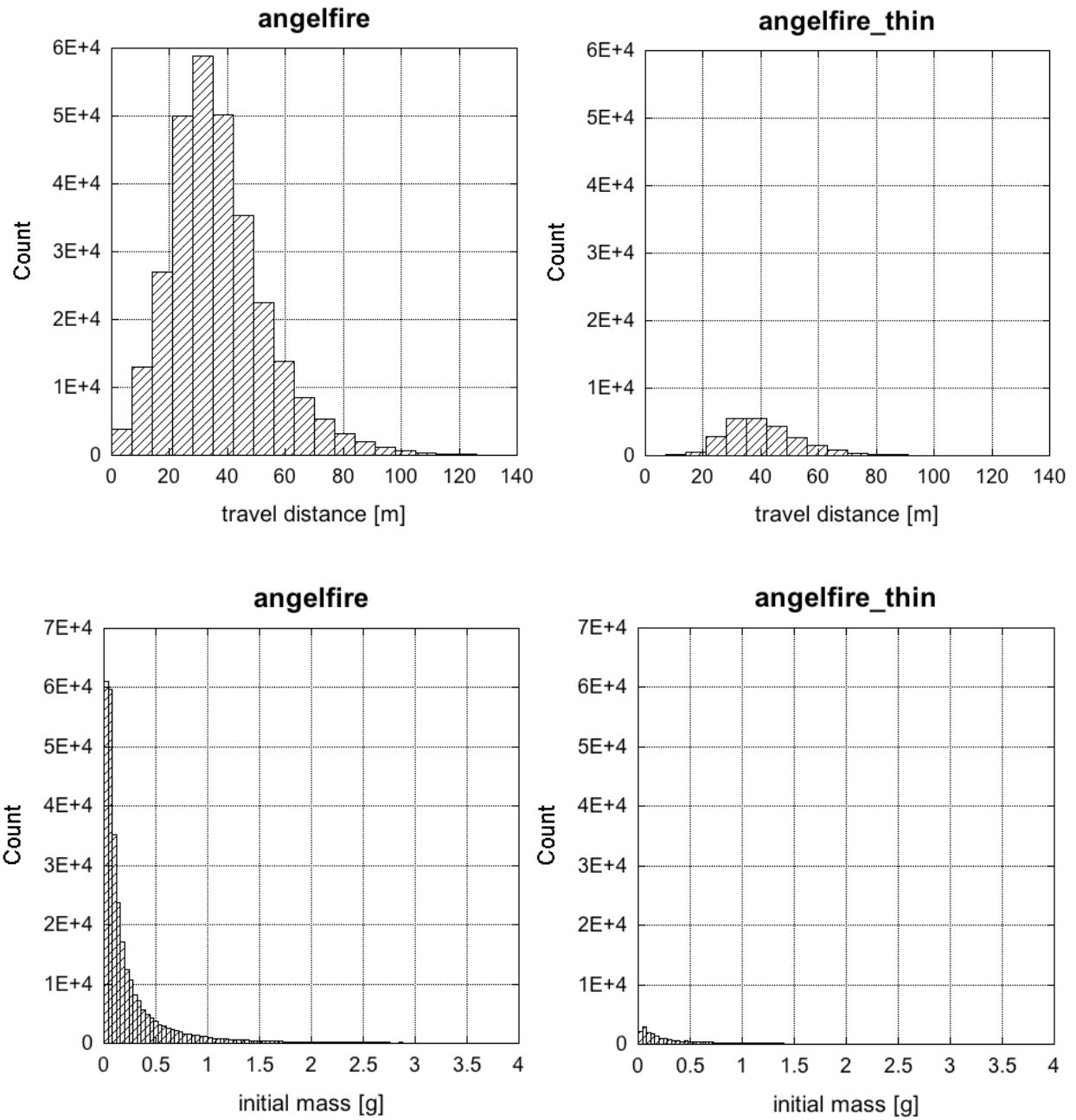


Figure 11. Histograms showing the number of brands launched corresponding to various travel distances and initial mass sizes.

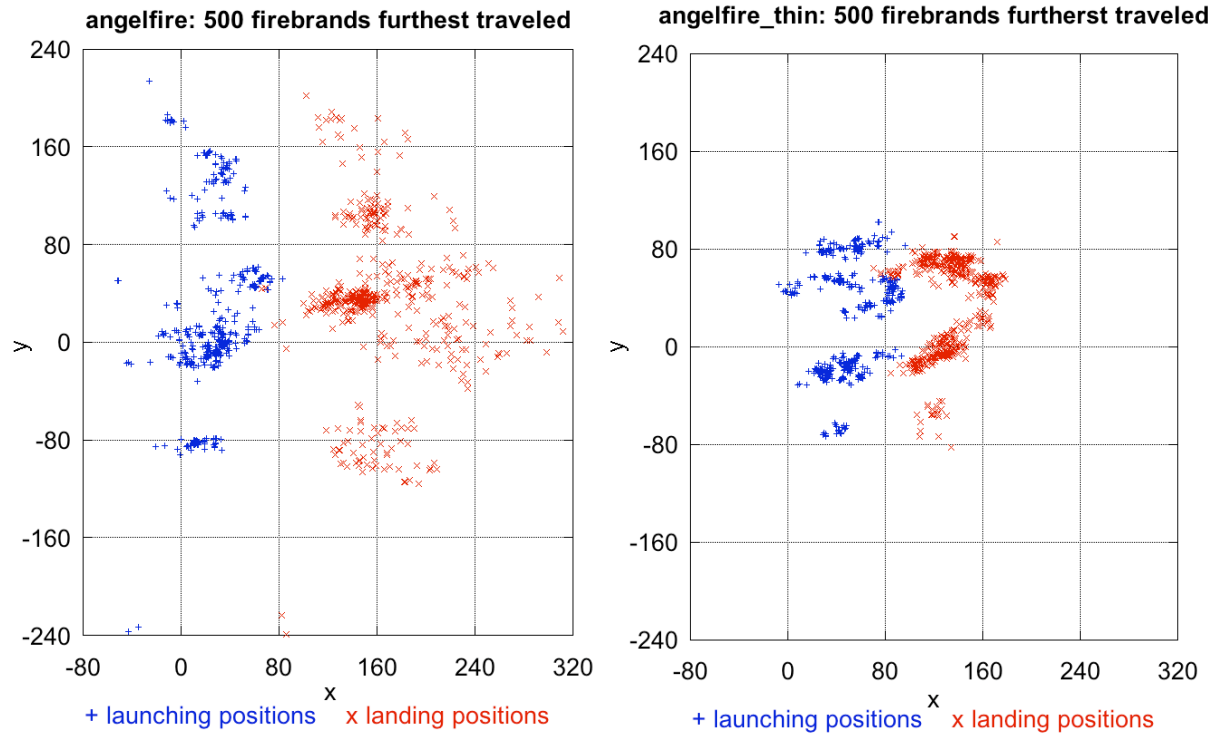


Figure 12. Maps showing launch and landing positions for 500 brands that travelled the farthest in each simulation.

D. Idealized complex terrains

Since topography and dynamic wind are indentified as critical factors in firebrand transport and flame/plume conditions, a study of topographic effects is currently in progress. Various idealized two-dimensional and three-dimensional hills and valleys are modeled.

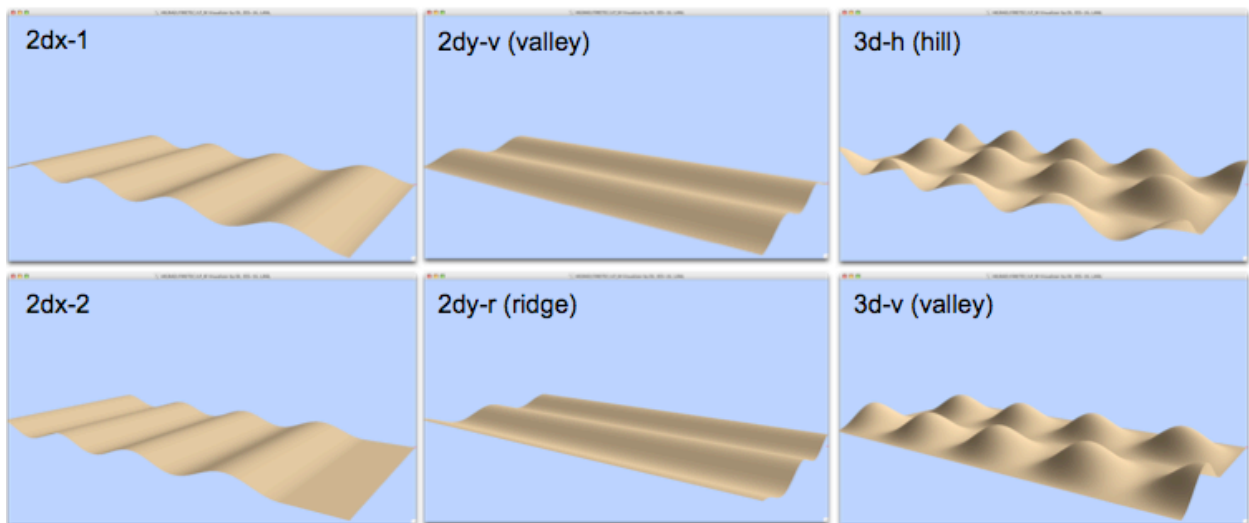


Figure 13. Idealized complex terrains used in firebrand simulations. Two- and three-dimensional hills and valleys are modeled.

Three-dimensional effects of wind flow around the fireline is found to be critical. Thus, the three-dimensional hill case (3d-h) had the most active firebrand behavior with the farthest travel distance and the largest number of firebrands lofted. Figure 14 shows the firebrand simulation of this case.

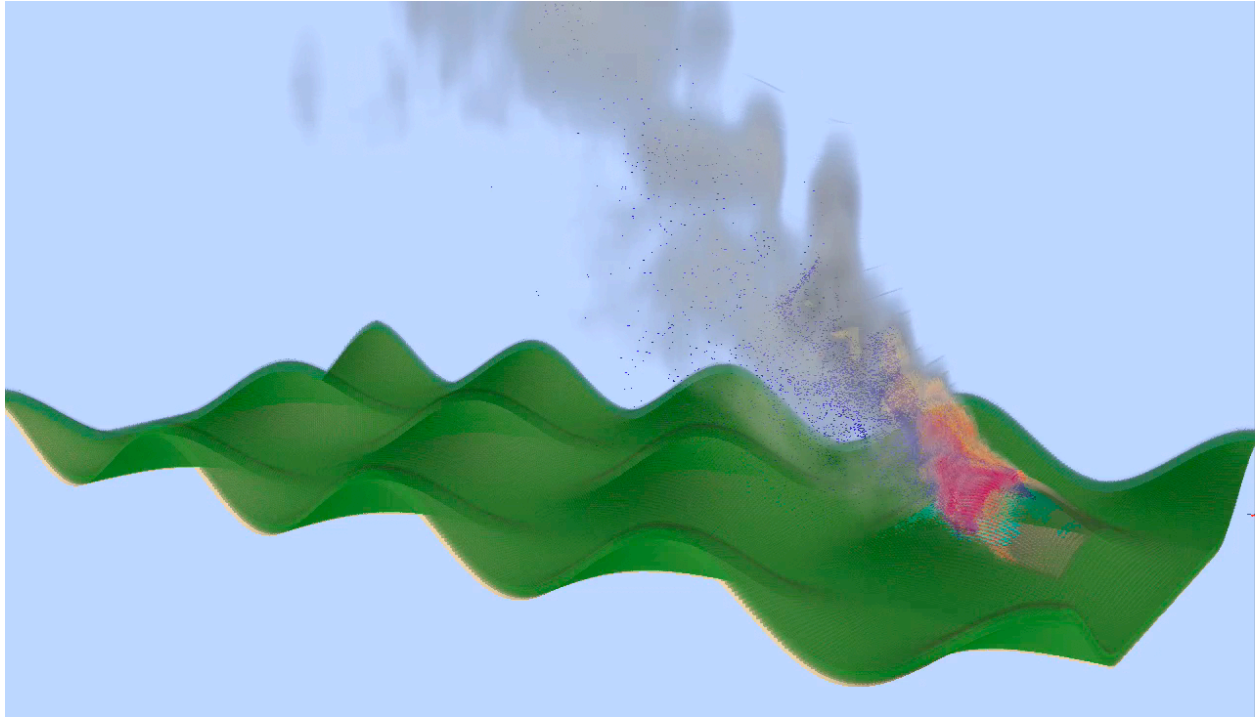


Figure 14. Firebrand simulation of 3-d hill case.

5. Management Implications

Firebrand behavior and spotting ignitions are difficult to quantitatively predict due to their stochastic nature. However, knowledge discovered through this study suggests that the followings factors should be taken into account for spotting ignitions.

A. Spotting distance/firebrand size and intensity/size of the fireZZ

A well-known characteristic of firebrand transport is that longer spotting distances are observed in larger fires because burning firebrands' lifetimes and spotting distances depend on the size of the firebrands. Stronger buoyant updrafts can loft larger firebrands that can achieve longer spotting distances, which is also affected by ambient wind. The size of the fire and its intensity generally determines how strong the buoyant plume is, and sometimes generates a fire whirl that has very strong updrafts. Following this reasoning, the maximum spotting distance has been used as a measure of spot fire hazard, and most firebrand models are based on this idea. This

study is not focused on developing another one-dimensional maximum spotting distance model since we found that three-dimensional flame/plume structures are also or even more important. However, the roles of the intensity and three-dimensional structure of the fire is very critical in lofting firebrands in our simulations, especially in the simulations on flat terrain. With the same length (100m) of initial fire line and the same terrain, the large differences in firebrand number/size/travel distance between canopy fires and surface fires are due to the aerial fuel and the vertical structure of the canopy inducing much stronger updrafts.

B. Flame and plume structure

As discussed in the previous section, flame and plume structures are found to be critical in firebrand phenomenon. Even in the cases of simple line fires on flat terrain, flame structure affected by entrainment plays a critical role, causing large numbers of firebrands of substantial sizes to be formed at the edges of the fire line as well toward the center of the crescent shape that the fire line forms due to differences in spread rate. In the simulations of sites in Las Vegas, NM and Angel Fire, NM with real topography and historical wind data, interactions between topography and the evolution of the fire line has been observed to be a critical factor in spotting behavior. It is suggested that understanding and predicting flame and plume structure formation while considering topographic effects is crucial to understand potential spot fires for fire managers.

C. Topography

Since topography is identified as one of the most critical factors in firebrand behavior, this study has focused on topographic effects. Actually, topography affects firebrand lofting and propagation indirectly: flame structure and local wind fields, which are heavily influenced by topographic features, determine contiguous fire spread rate and shape as well as plume structure. Firebrand lofting and propagation are driven by these fire features as well as the ambient wind field, which is also influenced by topography. In order to clarify these complex mechanisms, firebrand transport simulations have been performed with idealized complex terrain. From the simulations, one of the important findings is that the three-dimensional characteristics of topography are critical. For example, firebrand behavior in two-dimensional hills (ridges) and three-dimensional hills are significantly different since the wind flow patterns around the hills

and the fire line are quite different due to the three-dimensional flow effects. Thus, the three-dimensional topographic features are critical in spot fire phenomenon.

D. Dynamic wind (wind gust)

Firebrand simulations of ICFME were done using dynamic wind data that were measured in the field. Even though there was no significant spotting ignition in the ICFME burns, partly due to the firebreaks, the simulations show how dynamic wind fields affect contiguous fire spread, flame and plume structure, and eventually firebrand lofting and propagation. The ICFME burns and simulations were performed on flat terrain, and so the wind-gust effect in this simulation is separated from topographic effect. Complex terrain could induce local wind gusts, and the combined effect of topography and these wind gusts can create flame and plume structures that can drive strong firebrand activity.

E. Fuel condition

Hypothetical fires in Angel Fire, NM with thinned fuel and untreated fuel were simulated. Differences in firebrand activities between these fires were mainly observed in the number of firebrands lofted in the simulations, and thus a higher potential of spot fire ignition. If there is more fuel to burn, then surely there could be more firebrands lofted from this fuel. However, the fuel condition affects firebrand activity more than that, since the intensity and size of the fire drives the buoyancy of the flame and plume. In WUI fires, buildings are added fuel loadings for the fires. Firebrands produced in structural fires, such as firebrands from roof shingles, were observed in many large-scale WUI fires. (Pagni 1993; Wilson 1962) Thus, spotting fires should not be ignored in WUI fires.

In these discussions, the effects of topography, wind gusts and fuel conditions are all factors in the flame/plume structure of the main fire. Throughout this study, understanding the flame and plume structure of the fire was critical to understanding firebrand behavior.

6. Relationship with other recent findings

The project team has also been involved in large-scale urban fire simulations. The biggest difference between urban fire and wildfire are the fuel characteristics. Building material is mostly thermally thick while natural fuels in wildfire simulations are usually modeled as thermally thin since the main interest in wildfire simulations is the rate of spread, which is

primarily determined by thermally thin fuels. In preliminary simulations, it is found that the buoyancy of the urban fire could be stronger due to the fact that thermally thick fuels can burn longer, so the buoyant plume could have a stronger structure. The flame in urban fuel stays longer in one place, rather than spreading rapidly as in wildland fire fuels. This drives a stronger buoyant plume, which could produce more substantial firebrands. Moreover, the firebrands produced from structural fires could have a disk shape, which is more aerodynamically favorable for lofting and propagation than cylindrical shapes primarily found in wildfire fuels.

The project team has also been studying the effect of heterogeneity of fuel characteristics in wildfires, which is found to be a critical factor in fire spread and flame structure. In addition to differences between urban fuel and vegetation fuel characteristics, the integration and mixture of these fuels in a WUI region could provoke more active firebrand behavior than single wildfire fuels or single urban fire fuels.

Wind gusts and atmospheric turbulence is another topic the project team has been studying. The effect of high altitude atmospheric turbulence is expected to have more impact on discontinuous fire spread by firebrands than contiguous fire spread in surface and canopy fires.

7. Future work needed

Future work in firebrand investigations should relate to topics discussed in the previous section: modeling of urban fuel, fuel heterogeneity in WUI and atmospheric turbulence. More firebrand simulations to clarify topographic effect should continue. Since the flame and plume structure are found to be critical in firebrand behavior, more study of plume structure in wildland fires and WUI fires should be conducted. In addition to studying plume structures, the formation of fire whirls should be studied as a mechanism for firebrand lofting. The scale of the fire is an important factor in the plume structure and fire whirl formations, and so a future study should be conducted on various scales, focusing on larger scales than the simulations presented here ($> \sim 1$ km² domain).

The ignition mechanism of recipient fuel from landed firebrands should be studied. The ignition model is not incorporated with HIGRAD/FIRETEC_SPOT as yet. The main reason this ignition model is not yet incorporated is lack of knowledge of firebrand generation rates, i.e. how many

firebrands could be lofted, how frequently, etc.. In the current study, the generation rate in the simulations was chosen only to show the potential of firebrand lofting, considering computational efficiency. Since the firebrand phenomenon is another form of energy transfer from the burning fuels to the unburned fuels like other heat transfer mechanisms in fire spread, knowing how many firebrands with how much energy/mass are leaving the burning fuels is critical, and is not well understood.. Thus, an experimental/numerical study of firebrand generation rate is needed for future work.

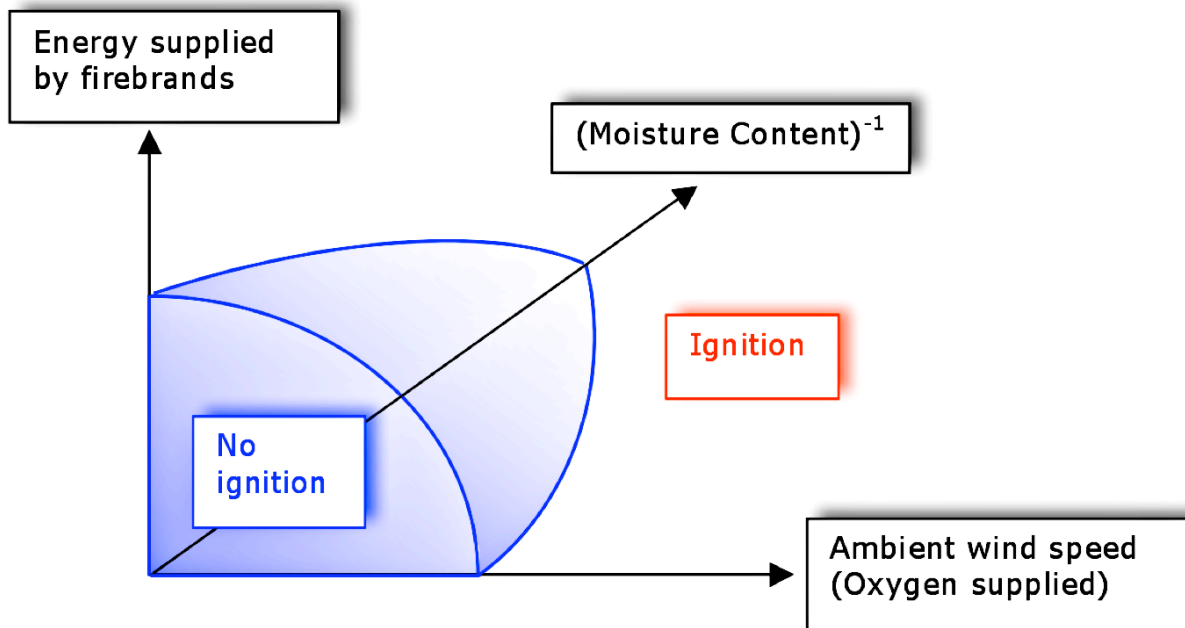


Figure 15. A qualitative map of ignition upon firebrand landing. Firebrand energy content, inverse moisture content, and ambient wind speed are set as axes. Near the origin, recipient fuel would not be ignited upon firebrand landing. Thus, ignition criteria may be expressed as a surface as shown in the map. Under the surface, fuel will be not ignited, and above the surface, fuel will be ignited.

Ignition of recipient fuels by a single firebrand should also be studied in terms of energy transfer. Figure 15 shows a qualitative map of ignition upon firebrand landing. The map is in the three-dimensional space consists of three major factors. In order to ignite the recipient fuel, the sufficient heat flux must exist for an adequate amount of time. The moisture content of both the recipient fuel and atmosphere are sinks of this heat flux to the recipient fuel, so this heat loss must be less than a certain amount for ignition. In order to maintain combustion (either glowing or flaming) of the landed firebrand during the ignition process, sufficient oxygen should be

supplied. The future study of the ignition of fuel by firebrands should be conducted from this basic concept.

8. The deliverables

A review paper about historical large-scale fires (urban and forest fires) and firebrand research, titled, “**Firebrands and Spotting Ignition in Large-Scale Fires**” has been accepted to the International Journal of Wildland Fires. A research paper about the firebrand models and simulations on flat terrain, “**Modeling Firebrand Transport in Wildfires using HIGRAD/FIRETEC**” has been submitted to the International Journal of Wildland Fire and is in the revision with positive reviews.

9. References

- Albini FA (1979) 'Spot fire distance from burning trees: A predictive model.' USDA Forest Service Intermountain Forest and Range Experiment Station INT-56, Ogden, Utah.
- Albini FA (1981) 'Spot fire distance from isolated sources: Extensions of a predictive model.' USDA Forest Service Intermountain Forest and Range Experiment Station, INT-309, Ogden, Utah.
- Albini FA (1982) Response of free-burning fires to non-steady wind. *Combustion science and technology* **29**, 225-241.
- Albini FA (1983a) 'Potential spotting distance from wind-driven surface fires.' USDA Forest Service Intermountain Forest and Range Experiment Station, Ogden, Utah.
- Albini FA (1983b) Transport of firebrands by line thermals. *Combustion Science and Technology* **32**, 277-288.
- Anderson HE (1983) 'Predicting wind-driven wild land fires size and shape.' USDA Forest Service Intermountain Forest and Range Experiment Station, Res. Pap. INT-305, Ogden, Utah.
- Butler BW, Bartlette RA, Bradshaw LS, Cohen JD, Andrews PL, Putnam T, Mangan RJ (1998) 'Fire behavior associated with the 1994 south canyon fire on storm king mountain, colorado.' USDA Forest Service Rocky Mountain Research Station, RMRS-RP-9, Ogden, UT
- Emmons H (1956) The film combustion of liquid fuel. *Zeitschrift für Angewandte Mathematik und Mechanik* **36**, 60-71.
- Fernandez-Pello AC (1982) Analysis of the forced convective burning of a combustible particle. *Combustion Science and Technology* **28**, 305-314.
- Fons WL (1946) Analysis of fire spread in light forest fuels. *Journal of Agricultural Research* **72**, 93-121.

- Himoto K, Tanaka T (2005) Transport of disk-shaped firebrands in a turbulent boundary layer. In 'the Eighth International Symposium on Fire Safety Science'. Beijing, China pp. 433-444. (International Association for Fire Safety Science)
- Hoerner SF (1958) 'Fluid-dynamic drag; practical information on aerodynamic drag and hydrodynamic resistance.' (Hoerner Fluid Dynamics: Midland Park, N. J.)
- Koo E (2008) 'Wildfire modeling.' (VDM Verlag)
- Koo E, Pagni PJ, Linn RR (2007) Using firetec to describe firebrand behavior in wildfires. In 'the Tenth International Symposium of Fire and Materials'. San Francisco, CA. (Interscience Communications)
- Lee SL, Hellman JM (1969) Study of firebrand trajectories in a turbulent swirling natural convection plume. *Combustion and Flame* **13**, 645-655.
- Lee SL, Hellman JM (1970) Firebrand trajectory study using an empirical velocity-dependent burning law. *Combustion and Flame* **15**, 265-273.
- Linn RR, Cunningham P (2005) Numerical simulations of grass fires using a coupled atmosphere–fire model: Basic fire behavior and dependence on wind speed. *Journal of Geophysical Research* **110**, D13107.
- Manzello SL, Maranghides A, Mell WE (2007) Firebrand generation from burning vegetation. *International Journal of Wildland Fire* **16**, 458-462.
- Muraszew A (1974) 'Firebrand phenomena.' The Aerospace Corp., No. ATR-74(8165-01)-1, El Segundo, CA.
- Muraszew A, Fedele JB (1976) 'Statistical model for spot fire hazard.' The Aerospace Corp., No. ATR-77(7588)-1, El Segundo, CA.
- Muraszew A, Fedele JB (1977) Trajectory of firebrands in and out of fire whirls. *Combustion and Flame* **30**, 321-324.
- Muraszew A, Fedele JB, Kuby WC (1975) 'Firebrand investigation.' The Aerospace Corp., No. ATR-75(7470)-1, El Segundo, CA.
- Pagni PJ (1981) Diffusion flame analyses. *Fire Safety Journal* **3**, 273-285.
- Pagni PJ (1993) Causes of the 20 october 1991 oakland-hills conflagration. *Fire Safety Journal* **21**, 331-339.
- Pimont F, Dupuy JL, Linn RR, Dupont S (2009) Validation of firetec wind-flows over a canopy and a fuel-break. *International Journal of Wildland Fire* **18**, 775-790.
- Spalding DB (1953) The combustion of liquid fuels. In 'Fourth Symposium on Combustion'. Cambridge, Massachusetts pp. 847-864. (The Combustion Institute)
- Tarifa CS, del Notario PP, Moreno FG (1965a) On flight paths and lifetimes of burning particles of wood. In 'Tenth Symposium on Combustion'. Pittsburgh, PA pp. 1021-1037. (The Combustion Institute)
- Tarifa CS, del Notario PP, Moreno FG, Villa AR (1967) 'Transport and combustion of firebrands.' Instituto Nacional de Tecnica Aeroespacial, Grants FG-SP-114, FG-SP-146, Madrid, Spain.

- Tarifa CS, del Notario PP, Villa AR, Martinez L, Perez O (1965b) 'Open fires and transport of firebrands.' Instituto Nacional de Tecnica Aeroespacial, Grants FG-SP-114, Madrid, Spain.
- Tse SD, Fernandez-Pello AC (1998) On the flight paths of metal particles and embers generated by power lines in high winds - a potential source of wildland fires. *Fire Safety Journal* **30**, 333-356.
- Turns SR (2000) 'An introduction to combustion : Concepts and applications.' (McGraw Hill: Boston)
- US National Park Service. (2000) 'Bandelier national monument cerro grande prescribed fire investigation report.' U.S. Dept. of the Interior National Park Service, Washington, D.C.
- White FM (1999) 'Fluid mechanics.' (WCB/McGraw-Hill: Boston)
- Wilson R (1962) 'The devil wind and wood shingles : The los angeles conflagration of 1961.' (National Fire Protection Association.: Boston)
- Woycheese JP (1996) Brand lofting in large scale fires. Thesis M S in Mechanical Engineering -- University of California Berkeley December 1996 thesis, University of California.
- Woycheese JP (2000) Brand lofting and propagation from large-scale fires. Thesis Ph D in Engineering-Mechanical Engineering --University of California Berkeley Spring 2000 thesis, University of California.
- Woycheese JP (2001) Wooden disk combustion for spot fire spread. In 'the Ninth International Fire Science and Engineering Conference (INTERFLAM)'. London, UK pp. 101-112. (Interscience Communications)
- Woycheese JP, Pagni PJ, Liepmann D (1998) Brand propagation from large-scale fires. In 'the Second International Conference of Fire Research and Engineering'. Gaithersburg, MD pp. 137-150. (Society of Fire Protection Engineers)
- Woycheese JP, Pagni PJ, Liepmann D (1999) Brand propagation from large-scale fires. *Journal of Fire Protection Engineering* **10**, 32-44.